

Lithological and Geomorphological Indicators of Glacial Genesis in the Upper Quaternary Strata, Nadym River Basin

Oleg Sizov¹, Anna Volvakh², Molodkov A.N.³, Andrey Vishnevskiy⁴, Andrey Soromotin⁵, and Evgeny Abakumov⁶

¹Oil and Gas Research Institute, Russian Academy of Sciences, Moscow, Russia

²Sobolev Institute of Geology and Mineralogy, Siberian Branch of Russian Academy of Sciences, Novosibirsk, Russia

³Tallin Technological University, Tallin, Estonia

⁴Novosibirsk State University, Novosibirsk, Russia

⁵Tyumen State University, Tyumen, Russia

⁶Saint-Petersburg State University, Saint Petersburg, Russia

Abstract

Analyzing the genesis of Quaternary sediments is important for understanding the glaciation history and development of marine sediments in the northern part of the Western Siberia. The problem is relevant since there is no consistent concept of the Quaternary sediments genesis in the north of Western Siberia. Their formation is associated with marine, glacial and interglacial sedimentation conditions. The research objective is to identify the persistent features characterizing the conditions of sedimentation and relief formation using the Nadym river basin as an example. The best method for studying this problem is a comprehensive analysis of the lithological, chronostratigraphic, petrographic and geomorphological studies of the Quaternary sediments upper strata. This study provides data from the analysis of the basic characteristics of quartz grains at the site. The rounding and morphology of the quartz grains provide evidence of possible glacial processing of some of the site strata. A petrographic study of selected boulder samples was performed. Some of them, by the shape and presence of hatching, can be attributed to glacial basins. The first use of a detailed digital elevation model applied to the study area made it possible to identify specific relief forms that could very likely be created during glaciations. Based on the analysis, we propose to consider the vast lake-alluvial plains in the Nadym river basin as periglacial regions. This idea lays the lithological framework for understanding the reasons for the formation of the modern landscape structure. The materials and descriptions provided are of interest to researchers of Quaternary sediments, topography, vegetation, and soil cover; particularly researchers engaged in revising the history of the natural environment development in the north of Western Siberia.

Keywords: Western Siberia, paleogeography, cover glaciation, Quaternary deposits, quartz grains, petrography, DEM

Introduction

The history of geomorphological development in the northern part of Western Siberia was a subject of intensive discussion at the end of the 20th century. The stratigraphy of the Yenisey river estuary is a key factor of the West-Siberian lowland quaternary evolution. Numerous examples of sedimentation alternation induced by various cover glaciations of different ages and thicknesses are presented. This series of sediments was used as a background for geological interpretation of the history of Western-Siberian lowland. The Q43 national geological map of Russia for this region indicates the dominance of glacial and fluvio-glacial types of the surface sediments (Alyavdin, Mokin, 1957.) The possible existence of ice sheets and related permafrost sediments was identified as a key issue at the beginning of the systematic

50 geological study of the territory in the 1960s. Some researchers (e.g., Svendsen,
51 2004) suggested that there were extensive glaciations that resulted in blocking the
52 river or some rivers at certain stages, leading to the formation of large glacier
53 dammed lakes (Grosvald, 1999.)

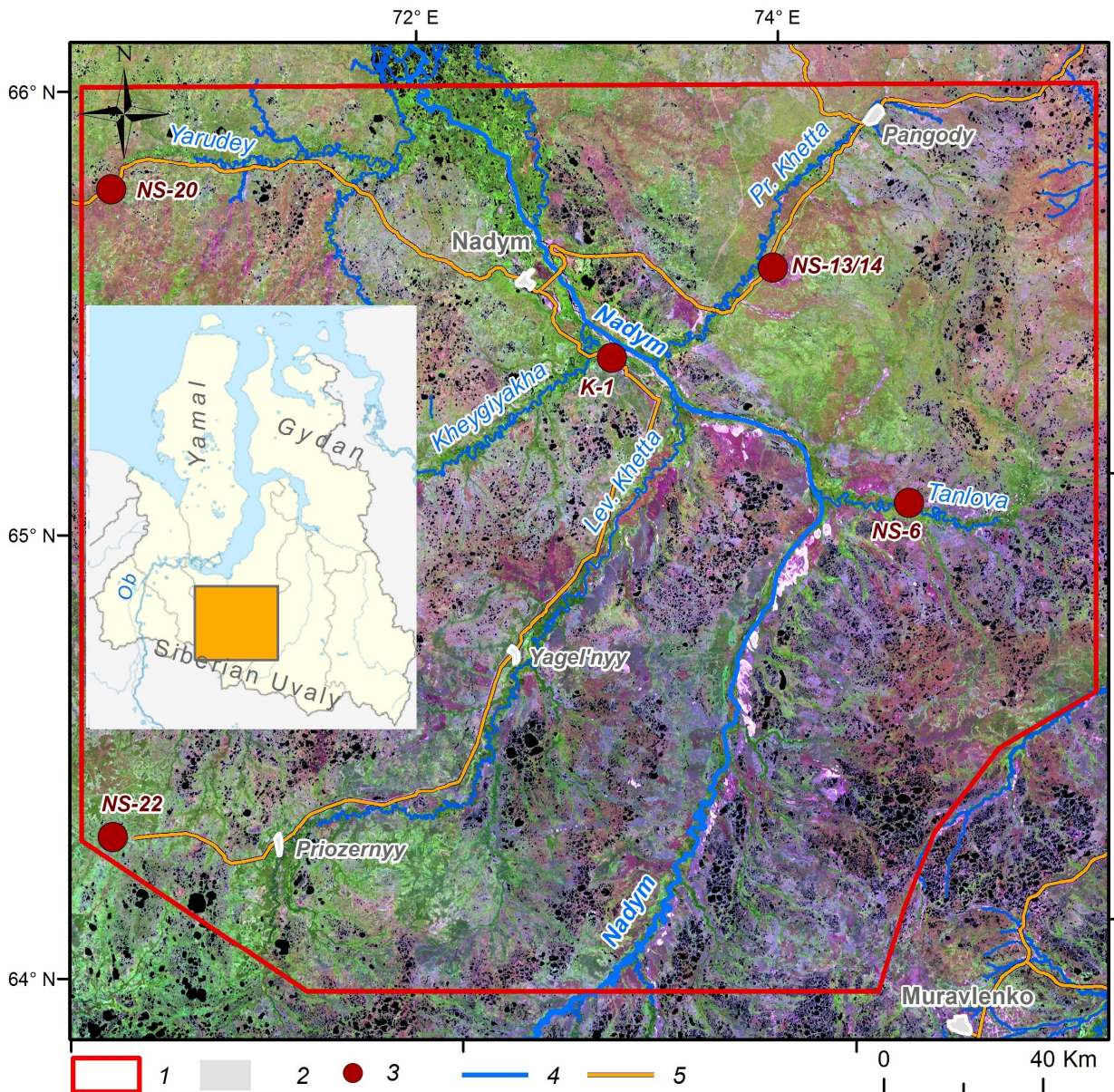
54 Another point of view considers possible glaciation on the plain (e.g.,
55 Generalov, 1986). It explains why the landforms are a sequence of terraces formed
56 by marine transgressions of various ages. There is also an opinion that the glaciation
57 was localized in the form of ice caps on separate watersheds and that the river flow
58 was unblocked (Velichko, 1987; Velichko et al., 1997.) Bolshiyarov (2006)
59 challenged this opinion and introduced the “passive glaciation” concept. In this
60 context, it is assumed that the sea level fluctuations might have created extensive
61 abrasion platforms. Another viewpoint suggests that the forms of relief which
62 previously were considered as glacial and fluvioglacial (morains and eskers), did
63 not originate from cover glaciations, but resulted from erosion, abrasion, and
64 thermokarst outcrops associated with permafrost-erosion and tectonic processes of
65 the late Pleistocene. It was suggested that isolated parts of Smarovskoye glaciation
66 existed in some areas of the Tyumen region combined with relics of ancient marine
67 terraces (Lazukov, 1972) Later, there was a heated discussion in the geology
68 community regarding the nature of possible glaciations and sedimentation history of
69 Western Siberia. It was suggested that glaciations extended up to Siberian ridges that
70 continued as the ancient periglacial Mansyiskoye lake (Grosvald, 1999)
71 Bolshiyarov (2006) suggested that the glaciations were passive, without forming a
72 discontinuous cover or preferential flow blocking in the area topography. At the
73 same time, the abrasion relief with extended ledges was formed in the late
74 Pleistocene period. Finally, the Q-42-43 national geological map suggests that there
75 is a combination of both terrestrial glacial and marine glacial sediments and
76 numerous lake terraces in Western Siberia. Nowadays, the glacial sediments are
77 excluded from the current version of the national geological map (Babushkin, 1995)
78 which in contradicts the results obtained by Astakhov et al. (2016) and Fredin et al.
79 (2012) Currently, there is no uniform concept of the landforms genesis in Western
80 Siberia. The basing of the Nadym River is considered as most important for the
81 Quaternary interpretation of the local Pleistocene history. The topography and
82 sediments of the Nadym River provide the most information for the study of glacial
83 landforms. Many field investigations and remote sensing operations were completed
84 by multiple generations of researchers, providing a valuable baseline for future
85 studies. The results of studying the Nadym River and adjacent areas, combined with
86 other data, served as a basis for a classification of the Quaternary deposits in West
87 Siberia (Maslennikov, 1998, Sedov et al, 2016, Sheinkman et al, 2016, Rusakov et
88 al, 2018.) Nevertheless, the current geological map (Faibusovic, Abakumova, 2015)
89 still has unsolved issues that are highlighted as new geological and geomorphologic
90 data are obtained.

91 The study objective is to summarize the results of detailed lithological,
92 chronostratigraphic, petrographic and geomorphological studies conducted in the
93 Nadym River basin, and to identify the origins of the key factors of sedimentation
94 accumulation and topography.

95
96
97
98
99
100
101
102
103
104
105
106

Materials and Methods

Fieldwork was conducted in 2016-2018 in the Nadym River Basin, including the valleys of its main tributaries: Heigiyaha (Longjuga), Jarudei, Tanlova, Left and Right Hetta. The region is characterized by a moderate human-induced burden. There are main gas pipelines (Urengoy-Pomara-Uzhhorod, Nadim-Punga-Lower Tura, etc.), high-voltage power transmission lines (200, 500 kV), an oil pipeline Yarudeyskoe field CGS to Puryel OPS), and the Nadym-Yagelskoye asphalt road. The survey covered the natural exposures along riverbanks, walls of dry quarries, as well as tops and slopes as the most informative terrain features. The background of this paper is the results of detailed studies of the five most prominent stratigraphy sections of the upper part of quaternary sediments (Figure 1, Table 1.)



107
108
109
110
111
112

Fig. 1. Overview map: 1: study area; 2: settlements; 3: studied and sampled locations; 4: waterways; 5: roads. Background image: Landsat 8, 2000.

113

Table 1

114

Site Properties

N	Coordinate s N, E	Elevation , a.s.l.	Geogenic location	Samplin g point location	Survey date	Thickness, m
K-1	65.351044 72.974041	24	Second above flood plain terrace	Eall of quarry	21.08.2016	4.2
NS-6	64.974808 74.499714	44	Second above flood plain terrace	River break	18.08.2017	9.5
NS - 13/1 4	65.52992 73.875985	44,5	Cam sediments	Top and lope of hill	22.08.2017	5.1
NS- 20	65.778072 70.29182	57	Easker sediments	The wall of quarry	11.08.2018	16
NS- 22	64.31688 70.232456	130	Watershed	The wall of quarry	13.08.2018	1.5

115

116

117

118

119

Samples for bulk chemical composition, grain size distribution, sand quartz grain morphoscopy and morphometry, as well as luminescent analysis of sandy textured particles of feldspars were taken from each specified layer of the studied sections in order to clarify the conditions of the sediment formation.

120

121

122

123

124

125

126

127

128

129

130

The bulk content of oxides was determined by the X-ray fluorescence method at the Analytical Center for Multi-Elemental and Isotope Research, Siberian Branch (SB), Russian Academy of Sciences (RAS), Novosibirsk, Russia, and at the laboratory of the Institute for Physical, Chemical and Biological Problems of Soil Science (Pushchino, Russia.) The grain size distribution was determined by conventional fractions separation (sieve analysis) of samples with the Fritsch Analysette 3 vibratory sieve shaker. The fractions were weighed with laboratory scales, 0.1 g accuracy. 2017 samples were analyzed at the Laboratory of Ground Mechanics, Institute of Cryosphere of the Earth, Tyumen Research Center, Russian Academy of Science with the Mastersizer 3000E laser diffraction particle size analyzer (Malvern Panalytical, Britain.)

131

132

133

134

135

136

137

138

139

140

141

142

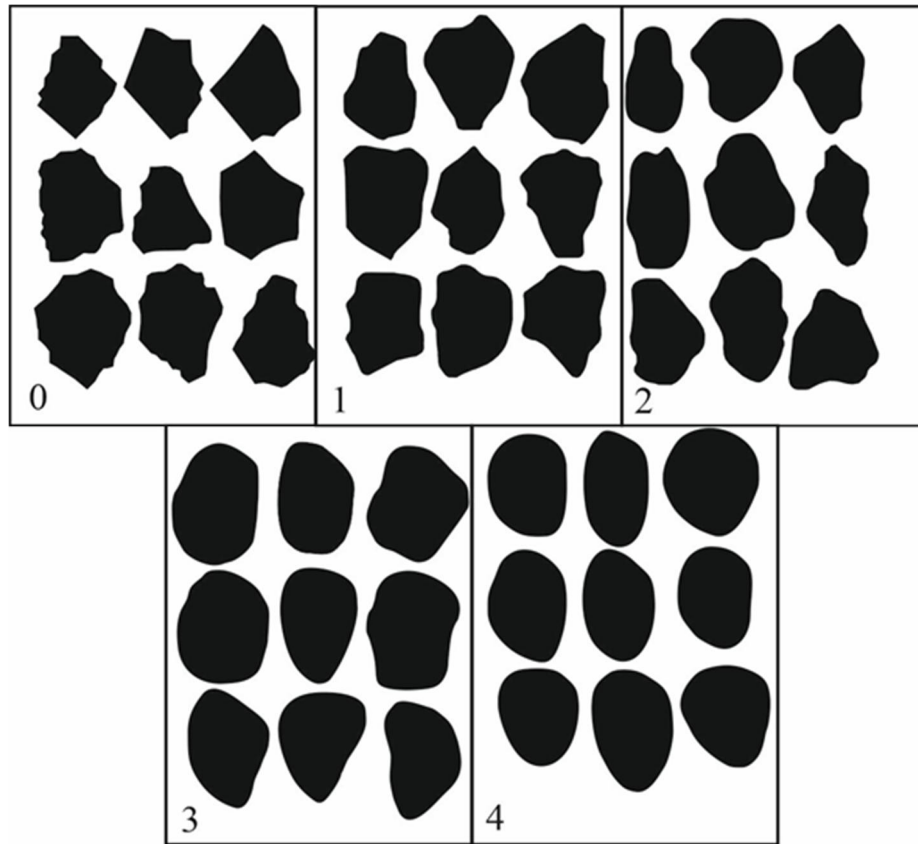
143

144

145

The Altami CM0870-T binocular microscope was used to study the quartz grains (50 grains per each sample) taken from the coarse sand fraction. The grain surface morphology was studied with the JEOL JSM-6510LV scanning electron microscope (SEM) using the secondary electron image (SEI) at the Analytical Center for Multi-Elemental and Isotope Research, SB, RAS. According to the technique applied (Velichko and Timireva, 1995), the grain scale was determined with L.B. Rukhin pattern (1969, Fig. 2) and A. V. Khabakov five-point scale (1946), where 0 is an untreated, and IV is a perfectly rounded grain. The coefficient of roundness and the grade of dullness (Velichko and Timireva, 1995) were estimated for each sample. The dullness of the grains was determined visually as glossy (shiny), quarter-matte, half-matte, and matte. The grain surface microrelief structure study was based on numerous published diagnostic features found in grains with various genesis and sediment accumulation conditions (e.g. Velichko, Timireva, 1995, Krinsley, Doornkamp, 2011; Vos et al., 2014; Woronko, 2016; Kalinska-Nartisa et al., 2017) The previous studies in Western Siberia that examined sand

146 quartz grain micromorphology covered peat histic sand deposits in the area of
147 Siberian Uvals, valleys of the rivers Taz and Pur, (Velichko et al., 2011) and aeolian
148 sediments of the southern part of Western Siberia (e.g. Sizikova, Zykina, 2015)
149



150
151 Fig. 2. Pattern for debris scale measurement (Rukhin, 1969)
152 0, 1, 2, 3, 4 are the classes of roundness (Khabakov, 1946)
153

154 The study of potassium feldspar grains, particularly, the determination of the
155 absolute age of the samples, used optically infrared-stimulated (IR-OSL) and
156 thermostimulated (TSL) luminescence (at the Lab of the Quaternary Period
157 Geochronology, Tallinn Technological University headed by A.N. Molodkov) The
158 IR-OSL measurements of the mineral grains extracted from the dating sample were
159 made at the laboratory with a special measurement system having a IR-OSL reader
160 as a primary instrument. The upper limit of the potassium feldspar-based IRSL
161 dating method is normally 300-500 ka, depending on burial conditions and the
162 physical properties of the mineral. The reliability of the dating technique used in this
163 study is demonstrated by several comparative results obtained through both
164 numerical dating methods (K-feldspar-based IRSL, mollusc shell-based electron
165 spin resonance (ESR), quartz-based optically stimulated afterglow (OSA), U-Th,
166 ¹⁴C) applied to the same sedimentary samples, and relative ones (Molodkov, 2012)
167 An overview of the IR-OSL dating procedure is presented by Molodkov and Bitinas
168 (2006)

169 In addition to the analysis at the sampling area, samples were taken for
170 petrographic examination. The samples were cut perpendicular to the lamination or
171 shaleness direction (if any) and made into transparent sections. The Carl Zeiss

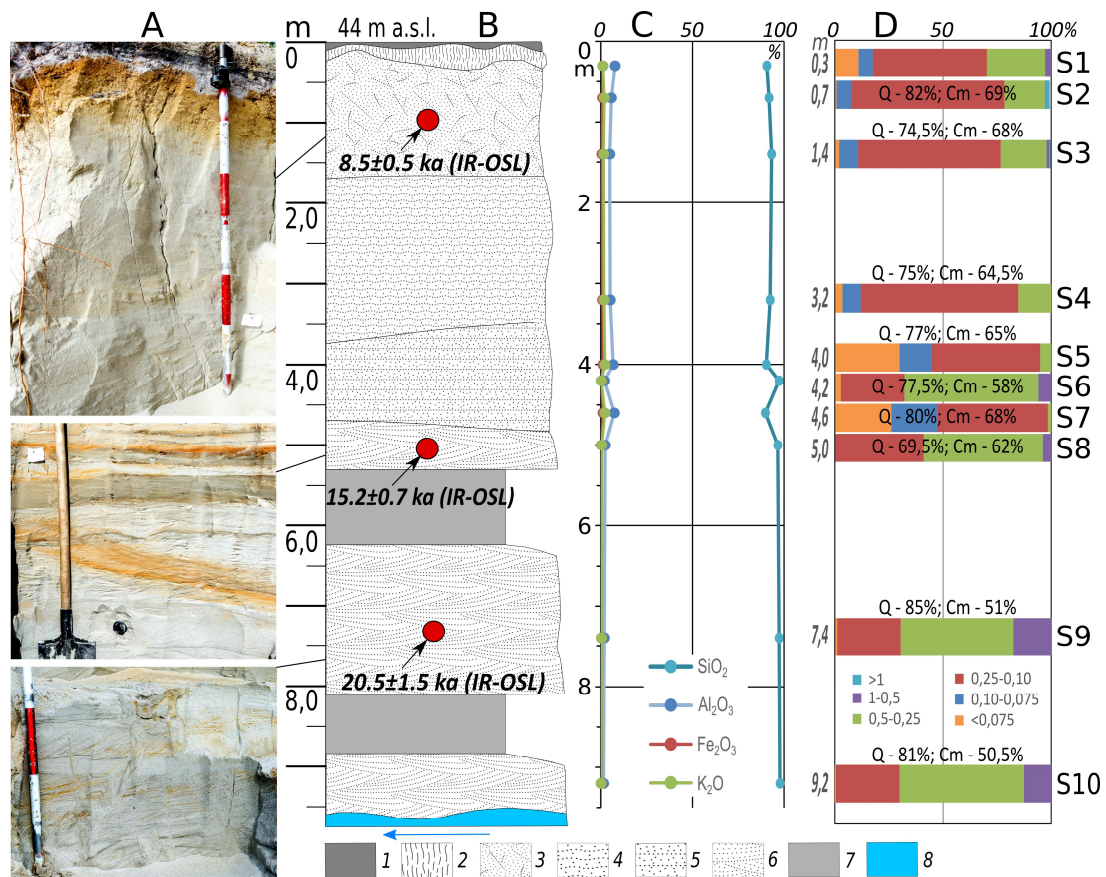
172 AxioScope A1 optical microscope at the Geology and Mineralogy Institute, SB
 173 RAS (Novosibirsk) was used.

174 For the first time for the studied area, digital terrain models (DTM) with
 175 spatial resolution of 12 and 26 m/px based on TerraSAR -X and TanDEM -X radar
 176 data were used to characterize the geomorphological structure. Baseline data were
 177 obtained from a research project supported by the Terrasar-X research team as part
 178 of activities to explore the potential of the TanDEM DTM for research
 179 (DEM_GEOL1378.) In addition, public multi-spectrum space images from Sentinel-
 180 2 (10 m/px.) were used to clarify the landscape boundaries.
 181 ([https://scihub.copernicus.eu/.](https://scihub.copernicus.eu/))

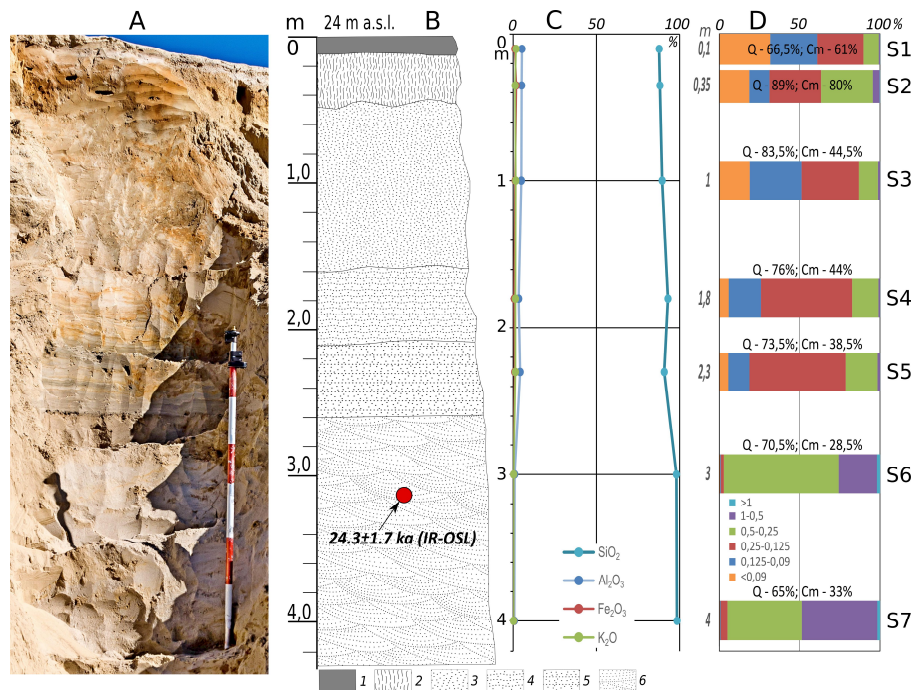
182 Results

183 Characteristics of the Sections

184
 185 The summary results of the quaternary sediment section study are shown in
 186 Figures 3-7 and Annexes 1, 2. From the data obtained, the following characteristic
 187 conditions of sediment accumulation can be distinguished:
 188
 189

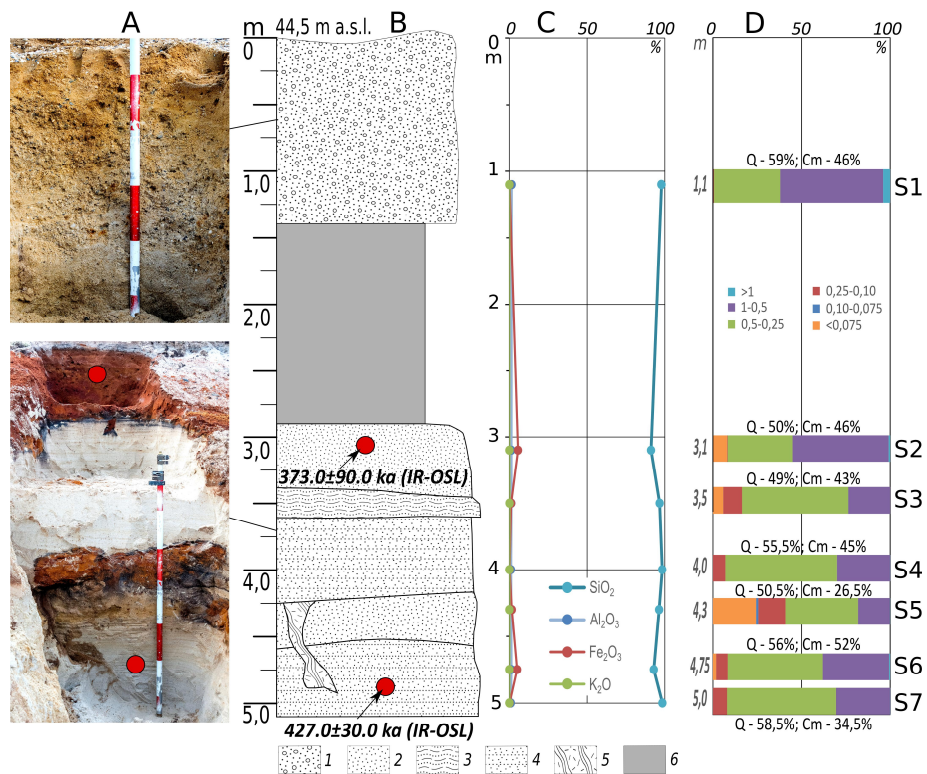


190
 191 Fig. 3. Summary results of research for NS-6 section. A: photographs (Sizov O.S., 2017); B:
 192 geological structure; C: bulk chemical data; D: grain size distribution (fractions, mm.) Symbols:
 193 1: podzol horizon of modern soil; 2: illivial-iron (spodic) horizon of modern soil; 3: sands without
 194 stratification; 4: undulating sand with secondary ironing; 5: horizontally layered sand with
 195 stratification of loam; 6: medium-and coarse-grained oblique sand; 7: colluvium; 8: river level;
 196 Q: coefficient of roundness of the sand quartz grains; Cm: degree of dullness; S: sample number.



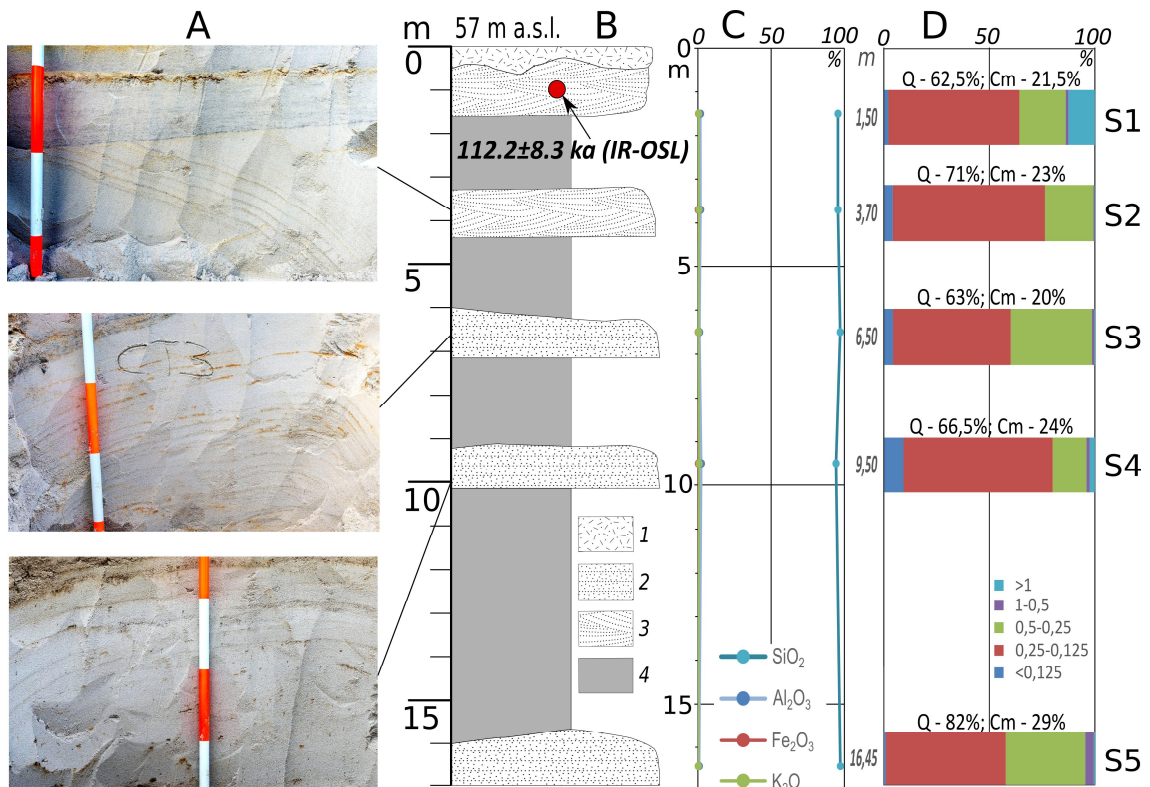
197
198
199
200
201
202
203
204
205

Fig. 4. Summary results of research for K-1 section: A: photographs (Sizov O.S., 2017); B: geological structure; C: bulk chemical data; D: grain size distribution (fractions, mm.) Symbols: 1: podzol horizon of modern soil; 2: illuvial-iron (spodic) horizon of modern soil; 3: sands without stratification; 4: undulating sand with secondary ironing; 5: horizontally layered sand with stratification of loam; 6: medium-and coarse-grained oblique sand; 7: colluvium; 8: river level; Q: coefficient of roundness of the sand quartz grains; Cm: degree of dullness; S: sample number.



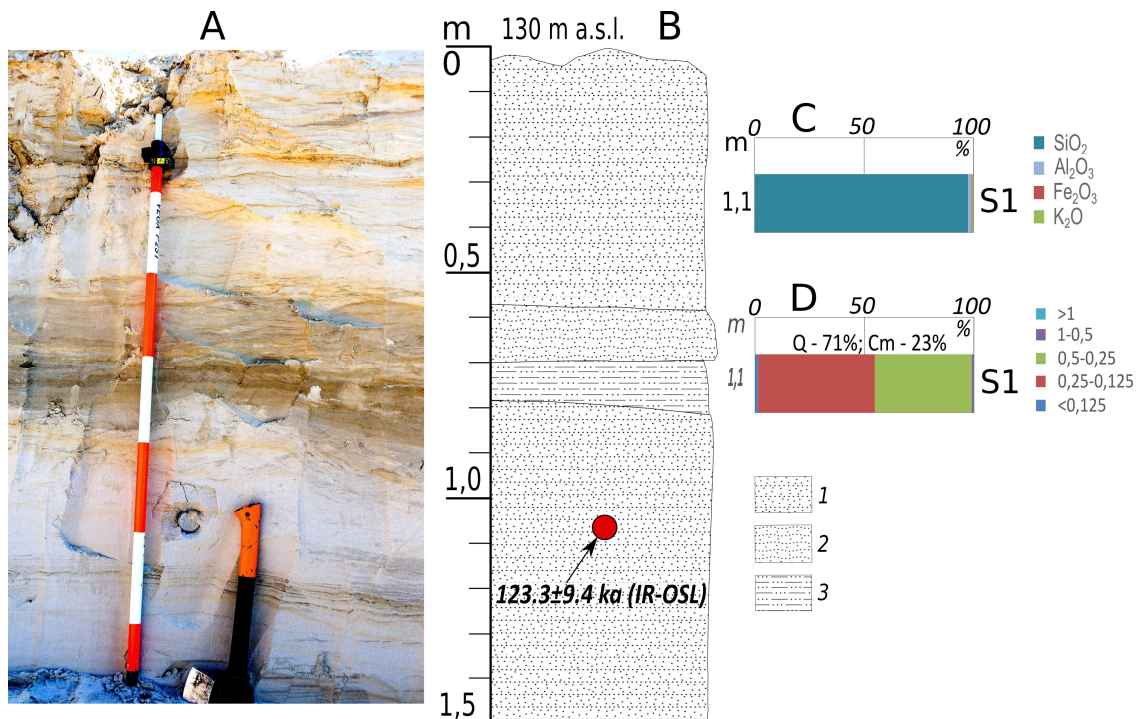
206
207
208
209
210
211

Fig. 5. Summary results of research for NS-13/14 section: A: photographs (Sizov O.S., 2017); B: geological structure; C: bulk chemical data; D: grain size distribution (fractions, mm.) Symbols: 1: coarse sand with pebbles; 2: unstratified red sand; 3: undulating black sand; 4: horizontally layered sand; 5: wedge filled by deposits of Layer 4; 6: colluviums; Q: coefficient of roundness of the sand quartz grain; Cm: degree of dullness; S: sample number.



212
213
214
215
216
217
218

Fig. 6. Summary results of research for section NS-20: A: photographs (Sizov O.S., 2017); B: geological structure; C: bulk chemical data; D: grain size distribution (fractions, mm.) Symbols: 1: overburden; 2: horizontally layered sand; 3: medium-and coarse-grained oblique sand; 4: colluvium; Q: coefficient of roundness of the sand quartz grains; Cm: degree of dullness; S: sample number.



219
220
221
222
223
224

Fig. 7. Summary results of research for section NS-22: A: photographs (Sizov O.S., 2017); B: geological structure; C: bulk chemical data; D: grain size distribution (fractions, mm.) Symbols: 1: horizontally layered grey sand; 2: oblique layered sand; 3: horizontally layered sandy loam; Q: coefficient of roundness of the sand quartz grain; Cm: degree of dullness; S: sample number.

225 1. Alluvial deposits predominate at the lower geomorphological level (up to
226 40-45 m.) Sections K-1 and NS-6 show the similar structure of the second above-
227 ground terrace of the Nadym and Tanlov rivers: in the upper part, thick podzolized
228 soil is formed over the aeolian deposits, in the middle part, floodplain type deposits
229 dominate, and in the lower part they are replaced by well-leached gray layered sand.
230 Down the profile, the SiO₂ content increases, while the content of other chemical
231 elements is low. The middle part of the section is dominated by fine and medium-
232 grained sand, the portion of large fractions increases in the lower part where single
233 pebbles up to 3-4 cm dia. are found. There are no permafrost-affected sediments.

234 2. At the middle geomorphological level, the sections show the structure of a
235 NS-13/14 kamiform hill and a linear-oriented relief (NS-20) The top of the hill is
236 covered with a solid layer of pebbles; at 1.2 m depth, it is followed by coarse sand.
237 Sandy deposits forming two distinct cycles are exposed in the middle part of the hill.
238 The unbroken red-colored sand is followed by black sand with slightly horizontal
239 orientation, which in turn is followed by light-grayish horizontally layered sand. In
240 the lower profile, the cycle is repeated; the difference is that the layer of intensively
241 reddish sand is not as thick. In the left lower part of the section, there is a frost wedge
242 microdepression, filled with the rock of layer S4. In general, the section is dominated
243 by medium- and coarse-grained sands of monomineral composition (the shares of
244 Fe, Al and other chemical elements are insignificant.)

245 In section NS-20, the slope of the extended elevation is exposed. It is
246 composed of a monotonic body of grey monomineral parallel and oblique-oriented
247 quartz sand. The sands throughout the section have an identical grey color and fine-
248 grained composition. The presence of thin iron-containing layers does not affect the
249 chemical composition of sediments: SiO₂ prevails in all layers. Local hills up to 5-
250 8 m high covered with large pebbles and boulders on the surface were found on the
251 top of the ridge along the survey path. In an exploration ditch on the top of the
252 microhill (1.5 m deep), large-grained non-grained sandy sediment with the
253 abundance of weakly rolled pebbles, gravel, and single large (up to 30-40 cm)
254 boulders were exposed. Their structure is similar to the deposits of the upper part of
255 section NS-13/14. In both sections, permafrost sediments and traces of frost cracking
256 are not found.

257 3. On the upper watershed geomorphological level NS2, sandy and pebble
258 deposits with the prevailing horizontal orientation were exposed on the flat slope of
259 the eastern cropping of the large local elevation. Sands in the sample are grey-
260 colored, fine and medium-grained. The SiO₂ content is 96.49%. A huge number of
261 large, weakly rolled boulders, up to 1.5 m in size, was found in the quarry and on
262 the sandbank of the nearest lake (100 m.)

263 It should be noted that grey fine, medium- and coarse-grained sands of
264 monomineral quartz composition are present in all sections (except for NS-13/14.)
265 In river terraces, such sands have oblique lamination, while on the watershed they are
266 reoriented horizontally. The sands have no permafrost features, cracking traces and,
267 in general, poor chemical composition. A landscape vegetation feature of such
268 sediments is pine sparse forests, which are able to grow on poor sandy soils with a
269 well-drained hydrologic behavior. Sandy soils lack organic materials and debris of

270 fossil clams, and do not show any salt content. Despite the presence of large debris
 271 on the scree slopes; boulders do not occur directly in the sands. Based on
 272 morphological, particle size and chemical features we believe that this type of sand
 273 sediment could be formed in subaquatic conditions in more severe environments as
 274 compared to modern climatic conditions. This is also confirmed by correlation
 275 coefficients value – quartz content is negative correlated with key oxides in bulk
 276 composition of the fine earth (Annex 2).

277

278 *Sediments Dating Results*

279 IR-OSL ages for the sediment samples from the sites studied and the related
 280 analytical data are listed in Table 2.

281

282 Table 2

283 Absolute dating by the IR-OSL method

Section	Sampling depth, m	Sample code	Age, years '000	U (ppm)	Th (ppm)	K (%)
K-1	3.15	RLQG 2443-057	24.3 ± 1.7	0.11	0.45	0.01
NS-6	1.0	RLQG 2563-019	8.5 ± 0.5	0.79	0.73	0.94
NS-6	5.0	RLQG 2564-118	15.2 ± 0.7	0.01	0.00	0.14
NS-6	7.3	RLQG 2565-118	20.5 ± 1.5	0.01	0.00	0.14
NS-13/14	3.1	RLQG 2567-019	373.0 ± 90.0	0.00	0.00	0.00
NS-13/14	4.9	RLQG 2568-019	427.0 ± 30.0	0.35	0.74	0.00
NS-20	1.1	RLQG 2577-059	112.2 ± 8.3	0.96	4.19	0.34
NS-22	1.0	RLQG 2578-059	123.3 ± 9.4	1.29	2.00	1.31

284

285 From section K-1, a single date of 24.3±1.7 (RLQG 2443-057) was obtained
 286 at the depth of 3.2 m. According to this age for the deposits studied there, its
 287 formation took place at the very end of the third (Lipovka-Novoselovo) warm phase,
 288 which was recorded in the north of Western Siberia during MIS 3 by both the ¹⁴C
 289 (Kind, 1974) and mollusc shell-based ESR (Molodkov, 2020) methods.

290 The normal sequence of the youngest ages of 20.5 ka (RLQG 2565-118), 15.2
 291 ka (RLQG 2564-118), and 8.5 ka (RLQG 2563-118) was obtained for section NS-6
 292 at the depths of 7.3 m, 5 m, and 1 m, respectively. Specific analytical features suggest
 293 the supply of the sedimentary rock from the same source area. The genesis of the
 294 deposits is also identical. It implies similar conditions for the rock transfer despite
 295 the likely difference in climatic conditions.

296 Somewhat unexpected were the dating results for two consecutive layers in
 297 section NS-13/14: 427.0 ka (RLQG 2567-119) and 373.0 ka (RLQG 2567-119).
 298 Finding very old Pleistocene deposits (MIS 11) is exceedingly rare. Judging from
 299 the analytics, the sedimentary rock in these layers came from different source areas
 300 and has fluvial, most likely river genesis. Under the given conditions of burial and
 301 physical properties of the mineral, the upper dating limit may be at least three times
 302 higher (i.e., up to about a million years.)

303 The last two datings at 123.3 ka (RLQG 2578-159) and 112.2 ka
 304 (RLQG 2577-159) were obtained from two sections: NS-22 and NS-20. They
 305 common feature is that both of them fall into MIS 5, as well as the fact that the

306 corresponding sedimentary rock also came from various source areas. The studied
307 sediments on the base of a group of key features are supposed to have fluvial (river
308 and lake) origin.

309

310 *Sand Quartz Grain Morphoscopy and Morphometry.*

311 Refer to Annexes 4-13 for the key results: coefficient of roundness, degrees
312 of dullness, and examples of the quartz grain appearance. The following is a brief
313 description of the main features.

314 NS-6. Aeolian genetic group. The upper part of the section (samples S2 and
315 S3) is characterized by a high coefficient of roundness (Q; 74.5 - 82%) and degree
316 of matting (Cm; 68 - 69%). IVth rounding class matte grains prevail; the complete
317 grain distribution vs. rounding and surface dullness are shown in Annex 4. The most
318 common element of grains microrelief in the S1 sample is a micro-pitted surface
319 (Annex 9 a, b), which is a feature of aeolian transportation (Velichko, Timireva,
320 1995.) Chemical etching is sometimes found in depressions. High coefficients of
321 roundness (Q) and degrees of dullness (Cm) along with the predominance of micro-
322 pitted grain texture suggest the dominance of aeolian processes during the
323 sedimentation. Several grains show signs of subaquatic treatment and origin in the
324 form of crescentic depressions and V-shapes percussions (refer to Annexes 9 a, b),
325 which preceded the aeolian stage. It seems to be associated with the accumulation
326 of rock from the river valleys.

327 For quartz grains from the floodplain deposits (samples S4, S5, S6, S7, S8),
328 the rounding coefficient (Q) is within the range of 65-80%; the degree of dullness
329 (Cm) is 58-68% (Fig. 3.) On the average, IV rounding class grains (Refer to Annex
330 4) with a half-matte surface prevailing in the samples. The number of completely
331 glossy grains increases (up to 22%). The entire grain surfaces have signs of
332 subaquatic processing: V-shaped percussions (Annex 9 d), often forming a fine-
333 pitted surface (Annex 9 c, d), and separate crescent gouges. Many grains show traces
334 of aeolian treatment, expressed as a micro-pitted texture (Annex 9 c), which
335 corresponds well to a sufficiently large share of matte grains in the sample. It can be
336 assumed that deposits of this layer are formed by fluvial river and aeolian processes
337 in the coastal environment.

338 For samples from the lower part of the section (samples S9, S10) Q = 81-85%
339 and Cm is 50.5-51%. Most grains belong to the IV rounding class. The number of
340 glossy grains (up to 32%) is significantly higher than in overlying sediments (refer
341 to Annex 4.) The primary grain treatment traces on the surface of all grains,
342 regardless of the roundness and dullness, are fine-pitted surfaces (Annex 9 e, f) and
343 individual well-developed V-shaped microdepressions (Annex 9 f), which is a sign
344 of active river fluvial transportation. There are grains of the II and III classes of
345 roundness; they differ from most grains by the presence of flat faces (Annex 9 g, h.)
346 The shapes of these grains resulted from the previous stages of grain treatment.
347 There are also signs of aqua treatment on its surfaces (Annex 9 g, h.)

348 The K-1 grain distribution across the section confirms the primary classification of
349 the section and matches well the morphometric and morphological properties of the
350 NS-6 section. Refer to Annex5 for the grain distribution by roundness and dullness.

351 Layer 6 (samples S6-S7) lying in the base of the section provides important
352 information. These samples differ in grain morphology from overlying sediments.
353 They are characterized by the lowest cross-sectional values of the coefficient of
354 roundness (63-65%) and the degree of mating (33-35%), the presence of glossy
355 grains in all classes of roundness (Annex 10), constrained or ground flat faces at
356 grains, and the development of sickle-like texture and fine pits on the grain surface.
357 With these features, it can be concluded that this layer was formed by fluvial
358 processes, but it should be emphasized that there is a rock in its composition that
359 may have been exposed to glacial processes in the past.

360 NS-13/14. For S1 deposits $Q = 59\%$, $C_m = 46\%$. Poor-rolled grains, class I
361 (32%) and medium-rounded grains, class II (24%) predominate. Most grains have
362 half-matte (34%) and quarter-matte (32%) surface (Annex 6.) The grains can be
363 categorized into two groups. The first group is represented by well-rounded mature
364 grains with a ubiquitous fine-pitted surface (Annex 11 a), which is a sign of
365 treatment by aqueous streams. In the second group, there are grains of irregular
366 shape (Annex 11 b), often with multiple or conchoidal fractures. The faces have
367 traces of treatment in subaquatic environment. Grains of the second group show
368 separate V-shaped and rarely crescentic-shaped percussions; their number and
369 location indicate a lower exposure to water flow. The presence of these two different
370 groups of grains suggests the ingress of rock from different sources, one of which
371 was the deposits with a poorly treated rock.

372 For underlying deposits (S2, S3, S4, S5, S6, S7) $Q = 49 - 58.5\%$, $C_m = 26.5 -$
373 52% . There, poorly-rounded and middle-rounded grains of classes I and II with a
374 glossy or quarter-matte surface prevail (Annex 6.) The grain surface is dominated
375 by traces of low-activity subaquatic treatment: V-shaped and crescentic
376 microdepressions (Annex 11 c-h.) Irregular grains with smooth surfaces are most
377 common, often with fractures (Annex 11 e, f, h), which probably indicates its arrival
378 from a source with poorly rounded materials. There are grains with conchoidal
379 fractures formed by desquamation processes due to grain freezing (Velichko,
380 Timireva, 1995) or under a big pressure applied to the grain (Immonen et al., 2014;
381 Vos et al., 2014) There are also V-shaped percussions along its surface, suggesting
382 that the deformation occurred before the last fluvial treatment. Many grains were
383 highly exposed to chemical processes expressed as etching through the depressions
384 on the grain and the Fe-Mn skins. The development of V-shaped forms only along
385 the protruding parts of the grain, a well-developed crescentic-shaped texture and
386 non-ubiquitous fine-pits, the average values of the coefficient of roundness and low
387 degrees of maturation suggest that the final processing of grains occurred in a
388 relatively calm aquatic environment. For S2 and S3 samples, in addition to traces of
389 subaquatic treatment, there are grains with small micro-pits (Annex 11 c, d), a sign
390 of aeolian treatment of grains.

391 NS-20. For samples S1, S2, S3, S4, S5, the coefficient of roundness (Q) is in
392 the range of 62.5-82%, the degree of dullness (C_m) is 20-29%. Glossy grains of II
393 and III classes of roundness prevail (Annex 7.) In the upper sediments (S1), there
394 are signs of aeolian treatment of grains expressed as micro-pits (Annex 12 a, b.)
395 However, they have a rather low value of C_m , which is not typical of aeolian

396 deposits. This suggests that the local aeolian redeposition of underlying sediments
397 occurred. The underlying layers (S2, S3, S4, S5) have sediment features; their
398 formation is probably associated with fluvio-glacial processes: the surface of most
399 grains is highly uneven, cavernous, and strongly mechanically deformed. These
400 properties can be found in glacial conditions (at the stages of previous processing.)
401 This is also suggested by the presence of deep-pits, grooves and parallel scratches
402 of various configurations (Annex 12 c, d, h.) The last agent in their treatment was a
403 subaquatic process, as indicated by frequently occurring V-shaped and crescentic
404 depressions (Annex 12 e, f, g.)

405 NS22. The coefficient of roundness (Q) is 79%, the degree of dullness (Cm)
406 is 31%. Most of the grains belong to class III of roundness, a slightly smaller number
407 of grains are of class IV; glossy grains prevail (Annex 8.) The morphology of the
408 grain surface is quite uniform and is mainly represented by grains with fine pits
409 covering the grain surface almost completely (Annex 13 a-f) or developed only on
410 microelevation parts of the grain (Annex 13 e, f.) This surface is a characteristic
411 feature of the long-term grain processing in a sufficiently active subaquatic
412 environment.

413

414 *Petrography*

415 The petrographic analysis of 15 samples taken in a quarry nearby the section
416 AS-3 (fig. 9, coordinates: N65.061417°, E72.943848°) enabled to distinguish
417 several groups of materials:

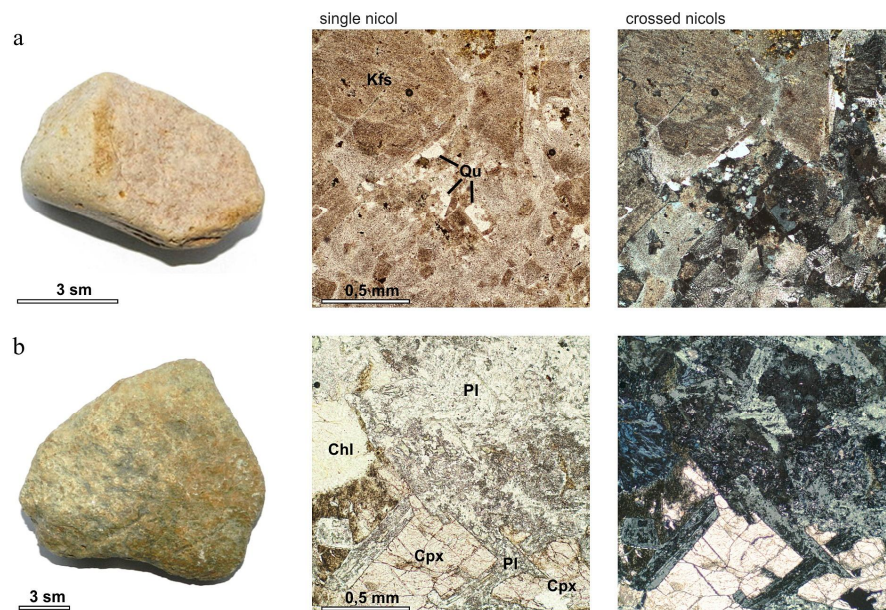
418 1) The first group (6 samples) is presented by grey, yellowish-grey, and
419 greenish-grey fine-grained and very fine-grained sandstone and siltstone with slab
420 jointing. They are usually moderately or poorly sorted and have primary foliation
421 that is emphasized by the regular orientation of flattened grains, varying grain size,
422 and matrix content. The matrix is hydromicaceous clay, sometimes with ferruginous
423 cement, with a small portion of silica. The fragments are usually sub-rounded or sub-
424 angular. The rock is composed of polymictic sandstones, similar to arkoses
425 sandstones. Quartz and feldspar prevail among the mineral grains, composing ~30
426 vol% of the fragments, while another third is predominantly composed of siliceous
427 rock fragments. Some samples contain significant amounts of muscovite (up to 5%
428 by volume), chlorite (including pseudomorphs after the dark-colored minerals), and
429 epidote. The presence of muscovite could be an indicator of low weathering of initial
430 sediments.

431 2) Pebbles and boulders of the second group of quartzitic and quartz sandstone
432 (6 samples) feature angular forms. The textures are usually massive and vary from
433 poorly to well sorted. The cement is predominantly quartz or quartz-
434 hydromicaceous, sometimes with goethite. The grain size varies greatly, but
435 medium-sized varieties prevail. More than 95% of grains are quartz and siliceous
436 lithoclasts, while muscovite, feldspar, epidote, zircon, monazite, and opaque
437 minerals are also present. The quartzitic sandstones show regenerative incrustations
438 around the primary rounded quartz grains. The grain boundaries are most often
439 irregular and frequently saw-shaped, which indicates a notable meta-genetic
440 alternation. Late veins of the fine-grained quartz aggregate are also rather frequent.

441 3) The third group of samples was the least numerous yet the most
442 informative. In this case, the first sample is a cobble of pinkish quartz trachyte–
443 alkaline intermediate volcanic rock. Large pelletized phenocrysts of potassic
444 feldspar (up to 1 cm) and rare fine quartz grains are distributed in the groundmass
445 composed of pelletized potassic feldspar and quartz (Figure 8(a).) Furthermore,
446 quartz-feldspathic myrmekites are rather frequent. There are small quantities of
447 plagioclase, dark-colored minerals that are substituted by aggregates of chlorite,
448 epidote, and opaque mineral.

449 The second sample is dolerite with typical poikilitic texture (Figure 8(b))
450 formed by large poikilitic clinopyroxene crystals (3-4 mm in diameter) with tabular
451 plagioclase (up to 1-1.5 mm.) There are large, separate hypidomorphic crystals of
452 basaltic hornblende (up to 2 mm), which are substituted by hydrous ferric oxides,
453 titanite, and chlorite. The main groundmass contains plagioclase and significant
454 amounts of chlorite, which is presumably a product of substitution of the volcanic
455 glass or clinopyroxene microliths.

456 The third sample is zoisite-amphibolite (zoisite-actinolite) metasomatic rock.
457 Light-green idiomorphic grains of amphibole prevail over hypidomorphic crystals
458 and sheaf-like aggregates of zoisite. Anhedral segregations of titanite and opaque
459 ore minerals are also present. From a general chemical perspective, it can be
460 suggested that the most probable protolith for this rock was a dolerite-like rock.
461

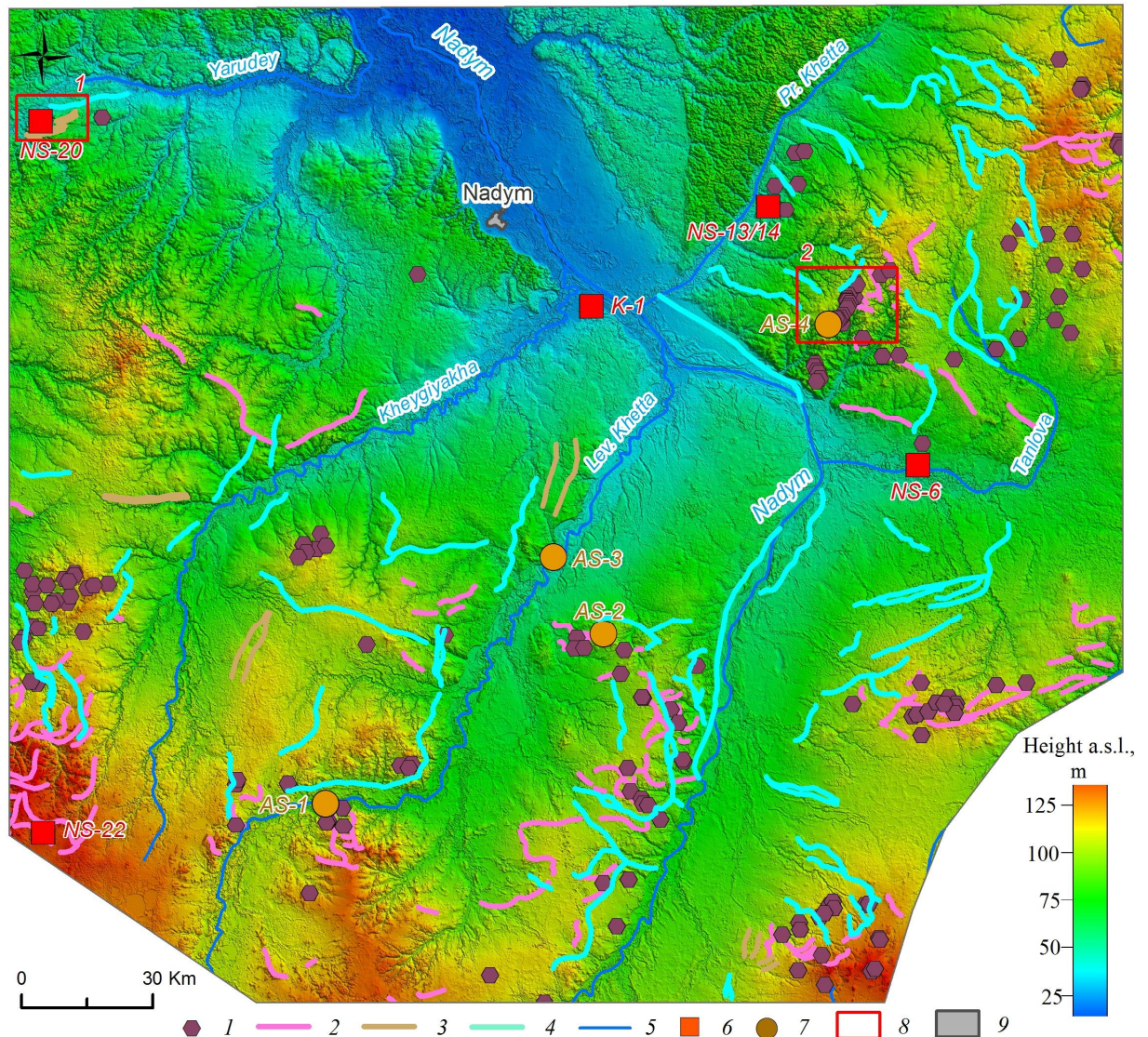


462
463 Figure 8. (a) Sample N-10 – pinkish quartz trachyte, large inclusions of potassic feldspar (Kfs)
464 with fine quartz grains (Qu) in the quartz-feldspathic matrix; (b) sample N-14: greenish-brown
465 dolerite, large poikilitic clinopyroxene crystals (Cpx) with thin plagioclase crystals (Pl), in the
466 groundmass: plagioclase chlorite (Chl.)
467

468 *Geomorphological Analysis*

469 The investigated area is in the zone of sparse northern taiga with extensive
470 peatlands. Therefore, the existing digital surface model (DSM), based on X-band
471 radar data with high penetration capacity, reflects in detail the terrain structure of
472 the territory. Based on the remote features available in the literature (Atkinson et al.,

473 2014; Astakhov et al., 2016) the DEM mapping of the glacial ice and fluvio-glacial
 474 relief features was performed using a site with an area of 54,117 sq. km as an
 475 example. Its boundaries run along the watershed of the Nadym River and its
 476 tributaries. The summary mapping results are shown in Figure 9 and Table 3.
 477



478
 479 Fig. 9. Results of the glacial and fluvio-glacial relief interpretation in the middle **course** of the
 480 Nadym River (the background image is a synthesized digital terrain model based on DEM
 481 TanDEM-X, 26 m resolution): 1: kame-like hummocks; 2: moraines; 3: parallel ridges; 4: valley
 482 trains; 5: waterways; 6: studied and sampled locations; 7: additional locations based on
 483 *Khlebnikov, 1954; Yevseyev, 1958*; 9: settlements

484
 485 Table 3
 486 Remote mapping of the glacial and fluvio-glacial relief features in the Nadym River basin (mid and
 487 lower courses)

Relief features	Number of identified objects	Total area/length, km
Kame-like hummocks	157	-
End moraines	122	851.3
Parallel ridges	16	157.2
Valley trains	103	1411.3

489 Based on the map obtained (Figure 9), it can be noted that the spread of the
490 assumed glacial and fluvioglacial relief features within the investigated area has two
491 distinct patterns:

492 – all identified features are to the south off the Jarudei and Pravaya Hetta
493 rivers, with individual objects found in the watershed between Jarudei and Heigiyahi
494 (Longjungan.) In the southern and western parts, the diversity and density of the
495 features are the highest (Tanlova and Pravaya Hetta rivers watershed, left bank of
496 the Nadym River in its middle course)

497 – all identified features are found at the heights from 40 m a.s.l. and higher;
498 the density of objects significantly increases in the watershed areas above 70-75 m.

499 The feature of the high elevation relief distribution is demonstrated by the
500 statistical data about the selected kameform hills. Among the 157 point objects, 145
501 (92%) are above 75 m, with 53 (34%) located within the narrow range of 95-104 m.
502 Below 75 m, large objects occur individually and are poorly distinguished
503 morphologically.

504 The network of extended (more than 850 km) proximal (kame) moraines that
505 mark the final glacial massif positions is confidently recognized. They have different
506 stretches (sub-latitudinal, north-western, etc.), which may indicate there was no
507 single direction of the cover glacial movement. In most cases, the moraines are
508 confined to the watersheds, while they are often accompanied by other glacial forms
509 (kames, postglacial rills, etc.) The chain of kame hills on the watershed of the
510 Tanlova and Pravaya Hetta Rivers are erosive remnants of the local moraine
511 formations, i.e. morphologically they occupy an intermediate position between the
512 individual moraines. On the watersheds, well-drained, dry areas of sand sands near
513 kame ridges are often subjected to deflation and active redispersal.

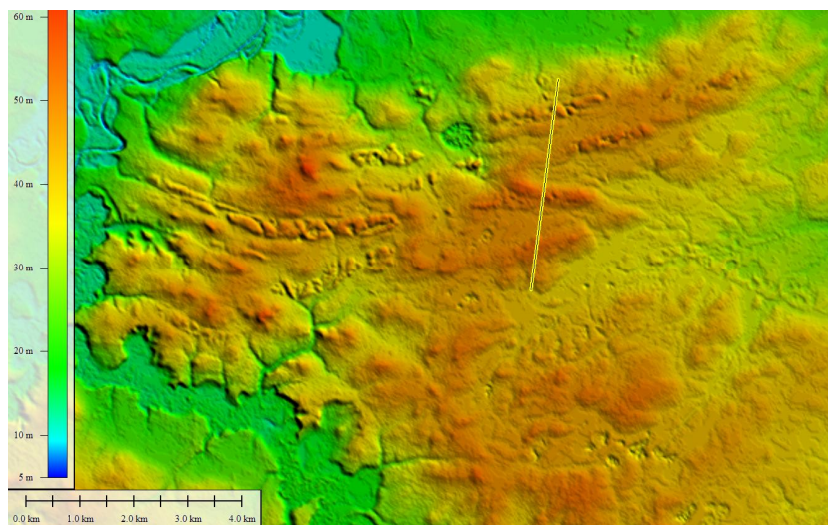
514 Some of the individual objects are linear ridges (about 157 km total length.)
515 The linear ridge relief also has visible signs of erosion (scours, rills, subsidences)
516 and in most cases can be traced as a specific linear landscape texture.

517 The valleys and rills of the melt glacial waters flow are more than 1,400 km
518 long. The valleys are well expressed in the southern and eastern parts of the study
519 area and are barely visible below 40 m asl. The network of valleys does not really
520 match the modern watercourses; they can be located both in parallel at a small
521 distance from the ancient valleys, or intersect them at right angles. The valleys and
522 hollows of the ancient runoff are often associated with terminal formations. The
523 preservation of valleys is one of the key signs of marine transgression absent in the
524 middle course of the Nadym River since the last glaciation of the region.

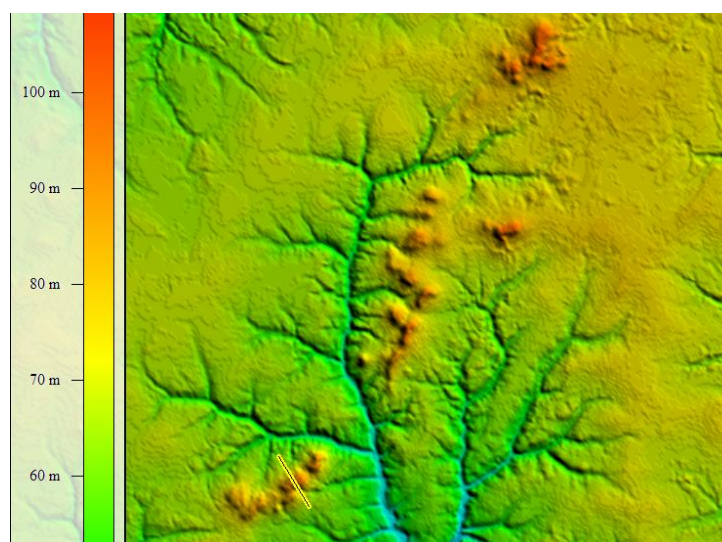
525 For clarity, two sections of typically glacial landforms are highlighted on the
526 map (Fig. 5):

527 1. A site with a predominant linear ridge relief, located on the right bank of
528 the Yarudey River (left tributary of the Nadym River), near the Nadym-Salekhard
529 highway under construction (Fig. 10.) Four long, curved ridges reaching a height of
530 55 m are well-preserved (the difference in relative heights is 10-12 m.) To the south
531 of the ridges stands a section of hilly, presumably kame, relief. The ridges are
532 complicated by thermokarst and erosion features.

533 2. The kame hill concentration site on the right bank of the Nadym River,
534 south of the main gas pipelines (Fig. 11.) The kames reach an absolute height of
535 more than 100 m (difference in relative height up to 30 m.) The kames are well
536 preserved despite the destruction of individual features by the river erosion.
537



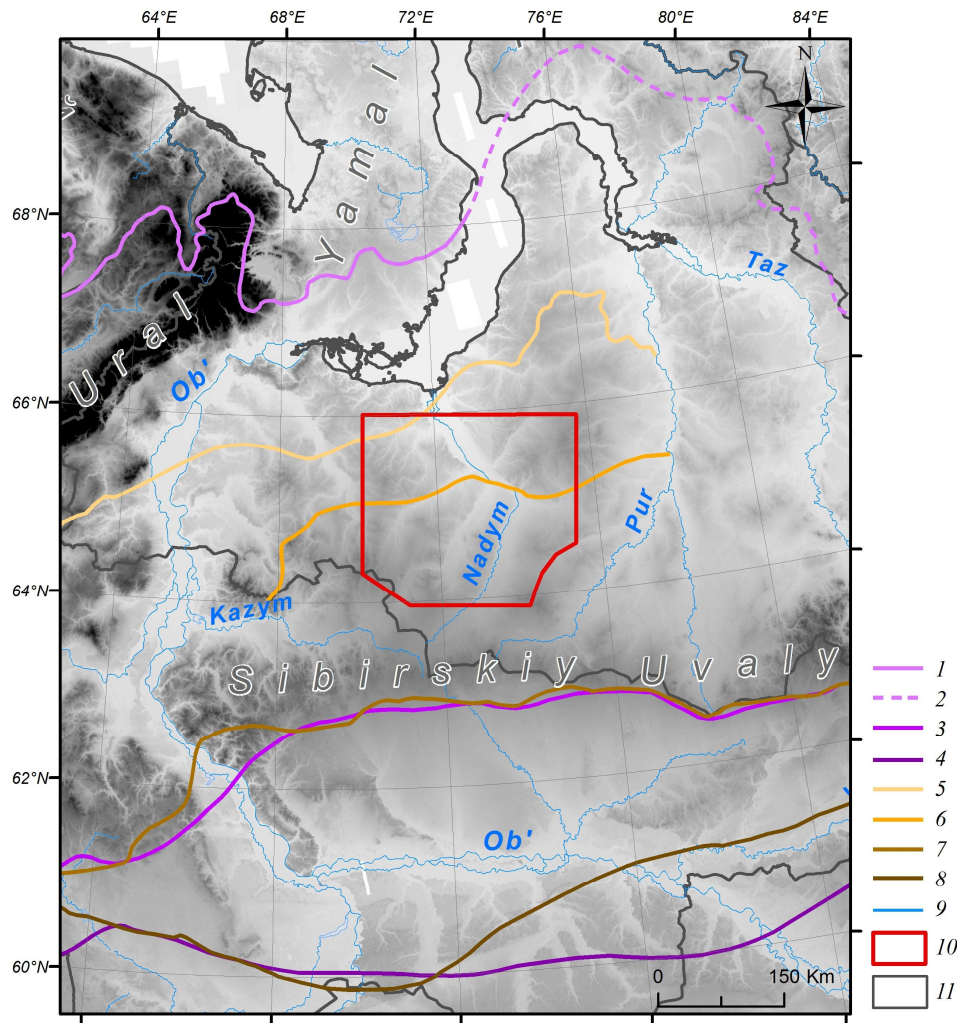
538
539 *Fig. 10. Parallel ridges, DEM TanDEM-X, 12 m / pixel*
540



541
542 *Fig. 11. Kame-like features, DEM TanDEM-X, 12 m / pixel.*
543

544 **Discussion**

545 According to current viewpoints, the territory of the north of Western Siberia
546 was exposed to several cover glaciations: Zyryanka (MIS4), Taz (MIS6) and
547 Samarovo (MIS8.) Areas at the lower level (up to 40-45 m a.s.l.) could represent
548 serial repeated marine transgressions in Kazantsev (MIS5) and Karga (MIS3) ages.
549 The glaciation boundary is presented in Figure 12, the chronological match of the
550 Western Siberian glaciation to the interglacial periods of the Eastern European
551 glaciation is presented in Figure 13. Directly within the boundaries of the
552 investigated areas, numerous researchers identified the boundaries of MIS6 stages
553 of Taz (MIS4) and possibly Zyryanka glaciation periods.
554



555
556
557
558
559
560
561

Fig. 12. 1-8: ice sheet boundaries (1: Zyryanka (Astakhov et al., 2016); 2: Zyryanka (assumed) (Astakhov et al., 2016); 3: Taz (Astakhov et al., 2016); 4: Samarovo (maximum) (Astakhov et al., 2016); 5: Zyryanka (Zemtsov, 1976; Babushkin, 1996); 6: Taz (second stage) (Zemtsov, 1976; Babushkin, 1996); 7: Taz (Zemtsov, 1976); 8: Samarovo (Zemtsov, 1976)); 9: water bodies; 10: study area; 11: administrative boundaries

Age (Ma)		East-European Plain	MIS	Western Siberia		
0		Holocene	1	Holocene		
0.1	LATE	Valdai cold warm cold	2	Sartanian cold		
			3	Karginian warm		
			4	Ermakovian(Zyrian) cold		
			5	Kazantsevo warm		
0.2	MIDDLE	Dnieper (Moscow) cold	6	Tazovian cold		
			7	Shirta warm		
			8	Samarovo cold		
					9	Tobolian warm
					11	
0.3	Chekalin warm	9	Tobolian warm			
				10		
0.4	Kaluga cold	10	Tobolian warm			
				11		
	Likhvin warm	11				

562
563
564
565

Рис. 13. Палеоэкологические сукцессии на Восточно-Европейской равнине (по Болыховской, 2004; Молдков и Болыховская, 2010) и в Западной Сибири (по Межрегиональной стратиграфической таблице..., 2014.)

566 The key natural feature of the glacial genesis of quaternary strata in northern
567 Western Siberia is the presence of wrecked rock: semi-rounded angular stones,
568 gravel and large boulders with evident glacial hatching, carried over by the glacier
569 from the territories outside the West Siberian Plain (Strelkov et al., 1965; Zemtsov,
570 1976) The water-glacial sediments in the research area include well-washed grey
571 sand characterized by poor chemical composition (the gravimetric concentration of
572 SiO₂ is 94-97%.) and also containing amendments of gravel and stones (Chekunova,
573 1954; Groysman, 1954; Khlebnikov, 1954.) The glacial sediments include unsorted
574 coarse-grained sands with an abundance of pebbles, as well as moraine-like bodies
575 of lumped clay, loam, and clay sand with gravel and large boulders. The petrographic
576 composition of boulders and pebbles includes quartz, opal, sandstones, quartz
577 porphyres, amphibolites, granitoids, gneises, trachites, etc. (Chekunova, 1954;
578 Groysman, 1954; Khlebnikov, 1954.) However, it was noted that interpreting the
579 exact location of the origin of these rocks from the geological markers representing
580 different territories is so far problematic.

581 The results of the study of the sections, in general, showed that the youngest
582 of the discussed sediments are those of the second floodplain terrace (section NS-6,
583 K-1.) In the top part, it includes aeolian sand formed no later than the beginning of
584 the Holocene (MIS1), in the middle part there are floodplain series of alluvium, in
585 the lower part there are river streams of grey oblique sand of the late MIS3 - middle
586 MIS 2.

587 The absolute age of the second floodplain terrace formation of the Nadym and
588 Tanlova Rivers (sections K-1 and NS-6) correlates well with numerous radiocarbon
589 and OSL datings of the second terrace throughout all the northern Western Siberia
590 (the age ranging from 42,000 to 25,000 years) (Nazarov, 2015) On average, the age
591 of the cover formation is between 20,000 and 12,000 years (Zemtsov, 1976;
592 Astakhov, 2006). Two types of glacial relief areas and extensive sandur surfaces
593 were identified on the surface of the second floodplain terrace in the large-scale field
594 studies on the left bank of the Left Kheta River (Vasilyev, 2007).

595 At the middle and upper geomorphological level, grey monomineral sand with
596 a similar age at the beginning of the NS-20 stage was also found in the NS-22 and
597 MIS5 sections. It can be suggested that during the Kazantsev interglacial period in
598 the vast area of the Nadym River basin there were favorable conditions for the
599 erosion of the previously accumulated sandy textured deposits and their transfer
600 downstream the main rivers.

601 One of the most interesting points of research is the kameform hill on the left
602 bank of the Right Hetta River (NS-13/14), the formation of its middle part
603 corresponds to the Tobol interglacial period (MIS9-11.) It can be suggested that the
604 sediments in the upper part of the hill are not younger than the Taz glaciation (MIS6),
605 while the pebble layer formed during the degradation of the glacier reinforced the
606 previous sediments and later was resistant to erosion, and was not covered by the
607 waters of the Kazantsev and Karga transgressions

608 The results of the sand quartz grain morphology analysis confirmed the
609 supposed genesis of the studied sections. Thus, for sections NS-6, K-1 it was shown
610 that in the upper part of sections there are aeolian sediments, below is floodplain

611 sand followed by fluvial sand. At the base of both sections, there are sediments in
612 which, apart from typically river grains, a large number of various morphology
613 grains are found. These are grains of varying degree of roundness, irregular shape
614 with a smooth surface and smooth faces, often on their surface, there are various
615 grooves and scratches formed under the strong mechanical impact, as well as
616 conchoidal fractures. Their origin could be a result of freezing weathering and
617 cryogenic transformation (Velichko, Timireva, 1995), as well as of high pressure
618 applied to the grain surface (Vos et al., 2014; Immonen et al., 2014.) Well-rounded
619 ellipsoid and ball-shaped grains predominate in the top layer sediments. One can
620 associate this distribution with materials coming from two different sources. One
621 source could have been the former glacial sediments eroded by fluvial processes.
622 This type of terrace structure corresponds well with the results of the study by
623 Velichko et al. (2011) who analyzed sands with underlay peat deposits in the
624 investigated region.

625 Quartz grains from sections NS13/14 and NS20 are often characterized by low
626 rounding classes, multiple conchoidal fractures, sometimes even conchoidal
627 systems, a deep-pitted surface, scratches, grooves, and cleavage surfaces. Such
628 elements could be signs of processes that occur in glacial environments. Often, there
629 are also signs of subsequent water treatment: separate crescentic depressions and
630 smoothed sharp peaks of grains. It indicates the redeposition of the glacial grains by
631 water flows. Along with the grains described above, there are also typical subaquatic
632 grains: well-rounded with a fine-pitted surface, but their number is inferior to grains
633 with glacial features.

634 Currently, we lack sufficient evidence to confirm the glacial genesis of these
635 deposits. It is possible that the grains were exposed to the effects of glacial processes,
636 with a final processing phase in their history that included subaquatic processes. In
637 section NS-22, the grain morphology provides evidence that suggests the existence
638 of a quiet subaquatic environment under which quartz grains underwent long-term
639 treatment.

640 In general, the results of sand quartz grain morphoscopy and morphometry
641 show that most quartz grains from all sections underwent complex multi-stage
642 processing throughout their life.

643 The petrographic diversity of erratic boulders in West Siberia helps us
644 distinguish two or three paleoglacial regions that combine several dozen distributed
645 provinces. Each is characterized by a specific set of rocks and petrographic features.
646 The first major generalization in this respect was made by Zemtsov (1976), who
647 identified the guide boulders of the Ural region as ultramafic and mafic rocks of the
648 Main (axial) Uralian zone, plagio-granites, and highly metamorphosed rocks
649 (gneisses and shales.) In the Central Siberian region, the prevailing boulders include
650 dolerites and basalts of the Putorana Plateau, as well as various granitoids, quartzites,
651 and Palaeozoic sandstones of the Taimyr Region. These studies were substantially
652 supplemented and detailed by a much more ambitious work by Sukhorukova et al.
653 (1987.)

654 Despite their small quantity, the petrographic analysis of pebbles and boulders
655 led to the following conclusions. First, high-silica alkaline effusive rocks (sample

656 N-10, quartz trachyte) are indicative of both the Northern Taimyr Province (Troitsky
657 & Shumilova, 1973) and many moraines of the Ural paleoglacial region
658 (Sukhorukova et al., 1987), but they are never found in the Putorana Plateau and the
659 southmost regions. Moreover, there is only a small relative share of dolerites (sample
660 N-14, dolerite) and other effusive mafic rocks, which is a property of Putorana and
661 Nizhnyaya Tunguska regions. In contrast, there is no limestone that would be typical
662 of the Central Siberian paleoglacial region (Kulyumbinsk and Sukhaya Tunguska
663 distributive provinces according to Sukhorukova et al., 1987.) However, there is no
664 granite in the samples either, which is a property of the Northern Taimyr region.

665 Second, quartz and quartzite sandstones are typical for the Ural paleoglacial
666 region, but their share is usually within a few per cent. Quartzitic sandstones also
667 described as Palaeozoic were found 50 km north of Surgut within the tentative
668 Central Siberian and Middle rock outwash zones (Sukhorukova et al., 1987.) The
669 source of the polymictic platy jointing sandstone could be the Palaeozoic bordering
670 of the eastern slope of the Urals (Sukhorukova et al., 1987) or the Mesozoic
671 sandstone of the West Siberian Plate.

672 In general, the samples have a significant proportion of terrigenous rocks
673 (sandstones and siltstones) and low content of dolerites. On the one hand, this can
674 be explained by the poor representativeness of the samples. Nevertheless, the key
675 washout zone could be located further north than the Putorana Plateau in the Taimyr
676 area. To substantiate this point of view, further research is planned to determine the
677 trace element composition and absolute dating and to expand the sampling.

678 Despite the numerous features that make it possible to attribute the thickness
679 of grey monomineral quartz sand (K-1, NS-6, NS-20) to fluvioglacial sediments,
680 and the upper pebble strata of section NS-13/14 to glacial sediments, the study did
681 not find typical moraine-like formations of lumped clay, loam and clay sand with
682 gravel and large boulders in this territory. However, detailed descriptions of this type
683 of sediment can be found in some references.

684 Thus, in the middle course of the Right Hetta River at Point 70 (Khlebnikov,
685 1954) 2.5 m deep there is a 20-meter layer of densely clumped loam with interlayers
686 of mica enriched sand (the layers are up to 25 cm wide) (section AS-1, Fig. 9.) The
687 color of the loam is brown-reddish-brown, small glitter mica is visible, and small
688 corners of debris (granite) are found, up to 25 cm in diameter. In the right part of the
689 section upstream, stripping exposed a layer of fine-grained sand. Below 15 m it is
690 followed by an interlayer of gravel-pebble rock. The prominent colluvium slope is
691 covered by loam crushed stone, and a cluster of gravel-pebble rock is also found on
692 the beaker. The huge kame moraine was described in the watershed of Nadym and
693 Levaya Hetta rivers (point 2368) (section AS-2, fig. 9) (Khlebnikov, 1954).

694 It has a wide extension and rises up to 25-30 m above the surrounding plain.
695 The ridge part of the range is convex and consists of individual peaks separated by
696 meso ridges. On the surface of the ridge, the congestion of pebble and gravel is
697 found. The gravel-pebble coarse-grained well-washed and leached sand is traced
698 down to the depth of 1.2 m.

699 Two esker-like linear elevations and a small kameform hill were discovered
700 in the lower course of the Right Hetta River at well No. 18 (Khlebnikov, 1954) at

701 1.8 m depth in the gravel-pebble horizon with a total depth of 17.6 m (section AS-3,
702 Fig. 9.) The diameters of the pebbles are between 0.5 and 3-4 cm. The pebbles are
703 not rolled and consist mainly of quartz and sandstone.

704 The moraine hills in the upper part of the Bolshoy Huhu River (right tributary
705 of the Nadym River) have a north-west and a north-east orientation. The length
706 reaches 6-7 km, and the relative height varies from 15 to 60 m. (Chekunova, 1954;
707 Yevseyev, 1958) morphologically, the steep slopes of the hills have individual
708 smoothed tops separated by small saddles. The upper layer of the hills to a depth of
709 1-2 m is peeled loam with abundant pebble rock. The pebbles are weak and poorly
710 rolled, and their diameters do not exceed 2-4 cm. Petrographic composition in one
711 of the sections reveals (so-called point 367 (Chekunova, 1954): silica, clay shale,
712 arkoses sandstones, breccia of clay-quartz rocks and limonite. The results of manual
713 drilling at some small hills (Yevseyev, 1958) (Yevseyev, 1958; Andreev, 1960)
714 showed that they are folded with permafrost sediments. The total ice content as
715 determined visually is not less than 30%. As an example, well No. 10 (Yevseyev,
716 1958), where light grey clay with yellowish color, light, porous, with alevrite
717 interlayers is found at a depth of 1.4-10.7 m, has a wavy and horizontal lamination
718 (section AS-4, Figure 9.) Clay thickness is underlayed with grey clay fine-grained
719 sands with poor sorting and admixture of gravel grains, quartz, and silicon pebbles.

720 Data from both our studies and previous field studies are in good
721 correspondence to the results of the analyses with the Tandem-X Digital Terrain
722 Models. These models revealed that despite the plain origin of the territory, the high
723 salinity and dominance of erosion processes, various glacial and fluvio-glacial relief
724 features preserved to various degrees (kameform hills, proximal moraines, and linear
725 elevations, glacial meltwaters etc.) are evident.

726 A linear-oriented relief caused by a glacial impact in northern Western Siberia
727 is highlighted on the Map of Quaternary Formations in Russia, 1:2,500,000 scale
728 (Astakhov, 2016.) At the same time, linear features and glacial remains are identified
729 on geological maps of larger scales (Babushkin, 1995.)

730 Nowadays, due to the increasing availability of initial DTM data, remote
731 mapping of glacial relief features become the standard method across the world
732 (Clark, 2004; Glasser, 2008; Sharpe, 2010; Atkinson, 2014; the Geological Surveys
733 in Canada and the United States, Norris, 2017.) Based on modern spatial data, a
734 detailed map for the British Isles Territory and Coastal Zone (BRITICE-2) is
735 available for digital study and analysis, and was updated (The BRITICE, 2017.) The
736 remote features of most forms of glacial relief for various natural conditions are
737 described in detail and offer numerous evidence that can be used as standards for
738 remote sensing data interpretation, including the entire north area of Western
739 Siberia.

740

741 ***Conclusions***

742 Our results showed high efficiency of simultaneous application of field
743 ground and remote methods even with limited raw site rocks. Sediments were
744 identified, which can be immediately attributed to fluvio-glacial (lower part of
745 section K-1 and NS-6, section NS-20) and glacial (upper layer of section NS-13/14)

746 origins. Traces of glacial treatment were also found as landforms in certain areas
747 such as kameform hills, proximal moraines, linear-bed elevations and depressions
748 of melt glacial water runoffs. Due to low organic substance content, sparse lichen-
749 pine trees are formed over the fluvio-glacial sediments on the low-fertile podzolic
750 soils. It is a characteristic landscape feature of the leaching soil condition for the
751 north taiga in Western Siberia. At the same time, the moraine-like layers of
752 aggregated clay, loam and clay sand with gravel and large stone boulders that could
753 not be found in field studies are widely described in stock sources previously
754 unpublished (particularly the Lion River Basin, Hetta and in the upper reaches of the
755 Great Huhu River.)

756 Thus, the development history of the Nadym River lower stream area provides
757 evidence that periods of cover glaciations occurred here in the Pleistocene. At the
758 same time, it is difficult to say whether it was a single glacier with a common front,
759 or whether there were several separate centers of ice accumulation. The available
760 data, especially the structure and functional characteristics of the relief, appear to
761 favor the second option, at least in the late Pleistocene. In the early periods, traces
762 of larger glaciation may represent the vast lake-alluvial plains and flood plains,
763 reaching a maximum area in the basin of the Nadym, Pur and Taz rivers. In this case,
764 they can be considered as the latest erosion formations but preserved a characteristic
765 structure inherited by modern landscapes.

766

767 *Acknowledgments*

768 The authors thank the Terrasar-X (DLR) research team for providing the
769 digital elevation models.

770 This study was funded by the RFBR and the Local Government of the Yamal-
771 Nenets Autonomous District, project No. 19-45-890008. The investigation is under
772 a public assignment by the Institute of Geology and Mineralogy, Siberian Branch,
773 Russian Academy of Sciences.

774

775 *References*

- 776 Alyavdin F.A., and Mokin N.P.: Geological map. 1rd ed. Scale 1:1,000,000. Ministry of Geology
777 and Subsoil Protection of the USSR, Map Q-43 (Novyy Port.) Gosgeoltekhizdat, Moscow,
778 1957.
- 779 Andreev Yu.F. About the relationship of linear-ridge topography with tectonic structures in the
780 north of Western Siberia (in the field of permafrost development.) *Geologiya i geokhimiya.*
781 *Geology and geochemistry*, 3(IX), 76–94, 1960.
- 782 Astakhov, V.I.: On chronostratigraphic units of the Upper Pleistocene in Siberia, *Geologiya i*
783 *geofizika*, 47(11), 1207–1220, 2006.
- 784 Astakhov V. Shkatova V., Zastrozhnov, A. and Chuyko, M.: Glacio-morphological Map of the
785 Russian Federation, *Quaternary International*, 420, 4–14, 2016.
- 786 Atkinson, N., Utting, D., and Pawley, S.: Landform signature of the Laurentide and Cordilleran
787 ice sheets across Alberta during the last glaciation. *Canadian Journal of Earth Sciences*,
788 51(12), 1067-1083, doi: 10.1139/cjes-2014-0112, 2014
- 789 Babushkin, A.E.: Quaternary map. 2rd ed. Scale 1:1,000,000. Russian Federation Committee on
790 Geology and Mining (Roskomnedra), Map Q-42,43 (Salekhard.) St. Petersburg: VSEGEI
791 Cartographic Factory, 1996.
- 792 Bolshiyarov, D.Yu.: Passive Glaciation of the Arctic and Antarctic Regions. AANII, Saint

- 793 Petersburg, 296 p, 2006.
- 794 Chekunova, V.S.: Geological and geomorphological survey of a part of the lower reaches of the
795 Nadym River basin and parts of the right bank of the Nadym Ob River. VSEGEI, Leningrad,
796 1954.
- 797 Clark, C, Evans, D, Khatwa, A., Bradwell, T., Jordan, C., Marsh, S., Mitchell, W., and Bateman,
798 M.: Map and GIS database of glacial landforms and features related to the last British ice
799 sheet. *Boreas*, 33, 359–375, 2004.
- 800 Bolikhovskaya, N. S.: Paleoenvironments and climato-stratigraphy of the loess-paleosol formation
801 of Northern Eurasia. *LOESSmFORM*, 4, 11–36, 2004.
- 802 Faibusovic, Ya. E. and Abakumova L.A. Map of Pliocene-Quaternary formations. 3rd ed. Scale
803 1:1,000,000. Federal Agency for Subsoil Use (Rosnedra), Map Q-43 (New Urengoy.) St.
804 Petersburg: VSEGEI Cartographic Factory, 2015.
- 805 Fredin, O., Rubensdotter L., Welden, A., Larsen, E. and Lysa, A.: Distribution of ice marginal
806 moraines in NW Russian, *Journal of Maps*, 8(3), 236–241, 2012. doi:
807 10.1080/17445647.2012.708536
- 808 Glasser, N., Jansson, K., Harrison, S., and Kleman, J.: The glacial geology and Pleistocene history
809 of South America between 38,8S and 56,8S. *Quaternary Science Reviews*, 27, 365–390,
810 2008.
- 811 Grosvald, M.G.: Eurasian Hydrospheric Catastrophes and Glaciations of the Arctic Region,
812 Nauchny Mir, Moscow, 1999.
- 813 Groysman, Ya.M.: Geological survey of the Haigi-Yakh River basin (Long-Yugan). VSEGEI,
814 Leningrad, 1954.
- 815 Generalov, P.P.: Upper Pleistocene of the lower course of the Ob River In: Collection of scientific
816 papers of the West Siberian Scientific and Research Geological Prospecting Petroleum
817 Institute, Tyumen, 56–77, 1986.
- 818 Immonen, N., Strand, K., Huusko, A., and Lunkka, J.P.: Imprint of late Pleistocene continental
819 processes visible in ice-rafted grains from the central Arctic ocean. *Quaternary Science
820 Reviews* 92, 133–139, 2014.
- 821 Interregional stratigraphic chart of the Quaternary of the territory of the Russian Federation.
822 Interdepartmental Stratigraphic Committee, VSEGEI, St. Petersburg, 2014.
- 823 Kalinska-Nartisa E., Woronko B., and Ning Wenxin. Microtextural inheritance on quartz sand
824 grains from Pleistocene periglacial environments of the Mazovian Lowland, Central Poland.
825 *Permafrost and Periglacial Processes* 28, 741–756, 2017.
- 826 Khabakov, A.V.: On roundness indexes of pebble, *Sovetskaya Geologiya*, 10, 98–99, 1946.
- 827 Khlebnikov, V.I.: Geological and geomorphological survey of a part of the middle reaches of the
828 Nadym river basin. VSEGEI, Leningrad, 1954.
- 829 Krinsley, D.H., and Doornkamp, J.C.: Atlas of quartz sand surface textures. 2nd edition.
830 Cambridge, Cambridge University Press, 102, 2011.
- 831 Kind, N.V.: Late Quaternary Geochronology According to Isotope Data. Nauka, Moscow, 1974.
- 832 Lazukov, G.I.: Antopogen of the northern part of Western Siberia (Paleogeography), Moscow, 127
833 p, 1972.
- 834 Maslennikov, V.V.: Regional Geo-Ecological Mapping at Scale of 1:1000000 Within the North
835 End of Tyumen Oblast. Labytnangi, 1998.
- 836 Molodkov, A.: The Late Pleistocene palaeoenvironmental evolution in Northern Eurasia through
837 the prism of the mollusc shell-based ESR dating evidence. *Quaternary International*, (in
838 press.), 2020.
- 839 Molodkov, A.: Cross-check of the dating results obtained by ESR and IR-OSL methods:
840 implication for the Pleistocene palaeoenvironmental reconstructions. *Quat. Geochronol.*, 10,
841 188–194, 2012.
- 842 Molodkov, A., and Bolikhovskaya, N.: Climato-chronostratigraphic framework of Pleistocene
843 terrestrial and marine deposits of Northern Eurasia based on pollen, electron spin resonance,

844 and infrared optically stimulated luminescence analyses. *Est. J. Earth Sci.* 59(1), 49–62,
845 2010.

846 Molodkov, A., and Bitinas, A.: Sedimentary record and luminescence chronology of the
847 Lateglacial and Holocene aeolian sediments in Lithuania. *Boreas*, 35 (2), 244–254, 2006.
848 Copernicus Open Access Hub (n.d.) Available at: <https://scihub.copernicus.eu/dhus/#/home>

849 Nazarov, D.V.: Upper Pleistocene in the northern end of Western Siberia. In: *Fundamental*
850 *problems of the Quaternary, results of the study and the main trends of further*
851 *research: Proceeding of the IX All-Russian Conference on Quaternary Research*, Sochava
852 *Institute of Geography of the SB RAS, Irkutsk*, 323–325, 2015.

853 Norris, S. L., Margold, M., and Froese, D.G.: Glacial landforms of northwest Saskatchewan.
854 *Journal of Maps*, 13, 600–607, doi:10.1080/17445647.2017.1342212, 2017.

855 Rukhin, L.B.: *Fundamentals of Lithology. Doctrine of Sedimentary Rocks*. Nedra, Leningrad,
856 1969.

857 Rusakov, A., Sedov, S., Sheinkman, V., Dobrynin, D., Zinovyev, E., Trofimova, S. and
858 Levchenko, S.: Late Pleistocene paleosols in the extra-glacial regions of Northwestern
859 Eurasia: Pedogenesis, post-pedogenic transformation, paleoenvironmental inferences.
860 *Quaternary International*. 501, 174–192, doi:10.1016/j.quaint.2018.03.020, 2018.

861 Sharpe, J., Sharpe, D., and Harris J.: A flowline map of glaciated Canada based on remote sensing
862 data. *Canadian Journal of Earth Sciences*, 47, 89–101, 2010.

863 Sedov, S., Rusakov, A., Sheinkman, V., and Korkka, M.: MIS3 paleosols in the center-north of
864 Eastern Europe and Western Siberia: Reductomorphic pedogenesis conditioned by
865 permafrost? *Catena*, 146, 38–47, doi:10.1016/j.catena.2016.03.022, 2016

866 Sheinkman, V., Sedov, S., Shumilovskikh, L., Korkina, E., Korokin, S., Zinovyev, E. and Golyeva,
867 A.: First results from the Late Pleistocene paleosols in northern Western Siberia:
868 Implications for pedogenesis and landscape evolution at the end of MIS3. *Quaternary*
869 *International*, 418, 132–146, doi:10.1016/j.quaint.2015.12.095, 2016.

870 Sizikova, A.O. and Zykina V.S.: The dynamics of the Late Pleistocene loess formation, Lozhok
871 section, Ob loess Plateau, SW Siberia. *Quaternary International*, 365, 4–14, 2015.

872 Strelkov S.A., Saks V.N., Arkhipov S.A., Volkova V.S. The problem of the Quaternary glaciations
873 of Siberia. The main problems of the study of the Quaternary period, Nauka, Moscow, 188–
874 205, 1965.

875 Svendsen, J.I., Alexanderson, H., Astakhov, V.I., Demidov, I., Dowdeswell J.A., and Funder S.:
876 Late Quaternary ice sheet history of Northern Eurasia. *Quaternary Science Reviews*, 23 (11–
877 13), 1229–1271, 2004.

878 Sukhorukova, S.S., Kostyuk M.A., Podsova, L.L., Babushkon A.E., Zolnikov, I.D., Abramova,
879 S.A. and Goncharov, S.V.: *Moraines and Dynamics of Glaciation in Western Siberia*. Works
880 of Institute of Geology and Geochemistry of the Siberian Branch of the USSR Academy of
881 Sciences, Issue 672. Nauka, Novosibirsk, 1987.

882 The BRITICE Glacial Mapping Project: version two release, 2017. Available at:
883 [https://shefuni.maps.arcgis.com/apps/webappviewer/index.html?id=fd78b03a74bb477c906](https://shefuni.maps.arcgis.com/apps/webappviewer/index.html?id=fd78b03a74bb477c906c5d4e0ba9abaf)
884 [c5d4e0ba9abaf](https://shefuni.maps.arcgis.com/apps/webappviewer/index.html?id=fd78b03a74bb477c906c5d4e0ba9abaf)

885 Troitskiy, S.L. and Shumilova, E.V.: Stratigraphy and Mineralogical-Petrographic Peculiarities of
886 Quaternary Deposits in the Vorontsov Yar Stratum in the Lower Course of the Yenisei River.
887 In: *Lithology and Conditions of Formation of the Quaternary Deposits of the Northern*
888 *Eurasia*, Institute of Geology and Geochemistry of the Siberian Branch of the USSR
889 *Academy of Sciences*, Novosibirsk, 5–37, 1974.

890 Vasilyev, S.V.: *Forest and Bog Landscapes of Western Siberia*. Izdatelstvo NTL, Tomsk, 2007.

891 Velichko, A.A. and Timireva S.N.: Morphoscopy and morphometry of quartz grains from loess
892 and buried soil layers, *GeoJournal*, 36(2/3), 143–149, 1995.

893 Velichko, A.A., Timireva, S.N., Kremenetski, K.V., McDonald, G.M. and Smith, L.C.: West
894 Siberian Plain as a late glacial desert, *Quaternary International*, 237 (1-2), 45–53, 2011.

895 Velichko, A.A.: Current state of conceptions on continental glaciers of the Earth. *Bulletin of the*

- 896 Academy of Sciences of the USSR, Geographical Series, 3, 21–34, 1987.
- 897 Velichko, A.A., Kononov, V.M. and Faustova M.A.: The last glaciation of Earth: size and volume
898 of ice-sheets, *Quaternary International*, 41 (42), 43–51, 1997.
- 899 Vos, K., Vandenberghe, N. and Elesen, J.: Surface textural analysis of quartz grains by scanning
900 electron microscopy (SEM): From sample preparation to environmental interpretation,
901 *Earth-Science Reviews*, 128, 93–104, 2014.
- 902 Woronko, B.: Frost weathering versus glacial grinding in the micromorphology of quartz sand
903 grains: Process and geological implications. *Sedimentary Geology*, 335, 103–119, 2016.
- 904 Zemtsov, A.A.: *Geomorphology of the West Siberian Plain (Northern and Central Parts)*,
905 Publishing house of the Tomsk State University, Tomsk, 1976.
- 906 Yevseyev, G.P., and Reynin, I.V.: *Geological structure and geomorphology of the Tanlova, Right
907 Khetta, and Big Huhu basins (right tributaries of the middle segment of the Nadym river).*
908 VNIGRI, Leningrad, 1958.

909 *Annexes*

910

911 Annex 1

912 Bulk content of chemical elements

Sampling depth, m	Sample No	Bulk content, %							
		SiO ₂	Al ₂ O ₃	Fe ₂ O ₃	K ₂ O	Na ₂ O	P ₂ O ₅	CaO	TiO ₂
K-1									
0.1	S1	87.65	5.27	0.95	1.66	1.00	0.03	0.51	0.64
0.35	S2	88.09	5.14	1.89	1.14	0.56	0.05	0.32	0.53
1	S3	89.49	4.93	1.20	1.52	0.75	0.04	0.41	0.41
1.8	S4	92.97	3.35	0.61	1.32	0.51	0.02	0.27	0.21
2.3	S5	90.71	4.21	0.92	1.35	0.64	0.03	0.38	0.39
3	S6	98.02	0.88	0.30	0.25	0.07	0.01	0.10	0.10
4	S7	98.39	0.69	0.25	0.20	<0.05	0.01	0.08	0.08
NS-6									
0.3	S1	90.60	6.20	0.87	0.91	0.63	0.08	0.28	0.37
0.7	S2	91.85	4.57	0.74	1.47	0.58	0.01	0.41	0.37
1.4	S3	93.22	3.92	0.51	1.15	0.57	0.01	0.31	0.25
3.2	S4	92.37	4.05	0.75	1.38	0.62	0.02	0.43	0.35
4	S5	90.32	5.39	0.98	1.74	0.62	0.02	0.46	0.47
4.2	S6	97.33	1.54	0.26	0.15	0.45	0.00	0.18	0.08
4.6	S7	89.79	5.86	0.95	1.80	0.65	0.03	0.63	0.35
5	S8	96.65	1.88	0.28	0.42	0.49	0.01	0.20	0.11
7.4	S9	97.29	1.46	0.24	0.25	0.48	0.01	0.16	0.07
9.2	S10	97.78	1.19	0.21	0.07	0.45	0.01	0.17	0.07
NS-13, 14									
1.1	S1	97.72	1.43	0.21	0.00	0.43	0.00	0.14	0.10
3.1	S2	91.00	1.26	5.62	0.00	0.63	1.28	0.16	0.07
3.5	S3	96.58	1.22	1.14	0.15	0.56	0.12	0.18	0.11
4	S4	98.14	0.99	0.15	0.00	0.48	0.00	0.15	0.07
4.3	S5	96.25	1.18	1.58	0.07	0.47	0.06	0.16	0.24
4.75	S6	92.75	1.23	5.08	0.01	0.64	0.02	0.18	0.12
5	S7	98.34	0.89	0.17	0.00	0.43	0.00	0.13	0.09
NS-20									
1.5	S1	95.61	1.79	0.39	0.48	0.08	0.02	0.08	0.44
3.7	S2	95.59	1.83	0.21	0.68	0.09	0.01	0.07	0.16
6.5	S3	97.12	1.14	0.19	0.39	0.09	0.01	0.07	0.10
9.5	S4	94.30	2.31	0.31	0.84	0.10	0.02	0.07	0.38
16.45	S5	97.26	0.93	0.22	0.22	0.05	0.01	0.07	0.20
NS-22									
1.1	S1	96.49	1.53	0.32	0.61	0.17	0.01	0.11	0.17

913

914

915 Annex 2

916 Spearman's coefficients of correlation

	SiO ₂	TiO ₂	Al ₂ O ₃	Fe ₂ O ₃	MnO	MgO	CaO	Na ₂ O	K ₂ O	P ₂ O ₅	BaO
SiO ₂	1	-1	-1	-0.89	-0.84	-0.76	-0.89	-0.89	-0.79	-0.81	-0.62
TiO ₂	-1	1	1	0.89	0.94	0.75	0.89	0.89	0.79	0.83	0.73
Al ₂ O ₃	-1	1	1	0.89	0.94	0.78	0.89	0.89	0.79	0.84	0.73
Fe ₂ O ₃	-0.89	0.89	0.89	1	0.93	0.95	0.75	0.75	0.61	0.97	0.61
MnO	-0.84	0.94	0.94	0.93	1	0.86	0.85	0.85	0.76	0.91	0.78
MgO	-0.76	0.78	0.78	0.95	0.86	1	0.67	0.67	0.52	0.99	0.54
CaO	-0.89	0.89	0.89	0.75	0.85	0.67	1	1	0.96	0.71	0.91
Na ₂ O	-0.89	0.89	0.89	0.75	0.85	0.67	1	1	0.96	0.71	0.91
K ₂ O	-0.79	0.79	0.79	0.61	0.76	0.52	0.96	0.96	1	0.56	0.96
P ₂ O ₅	-0.81	0.83	0.84	0.97	0.91	0.99	0.71	0.71	0.56	1	0.59
BaO	-0.62	0.73	0.73	0.61	0.78	0.54	0.91	0.91	0.96	0.59	1

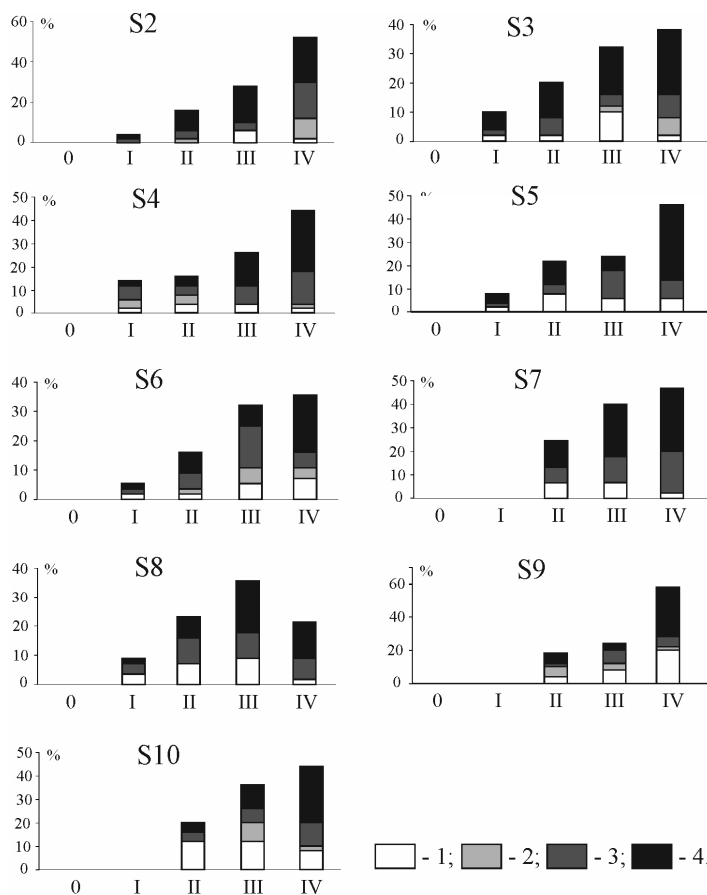
917 Significance level $p < 0.05$

918
919

Annex 3
Grain size distribution

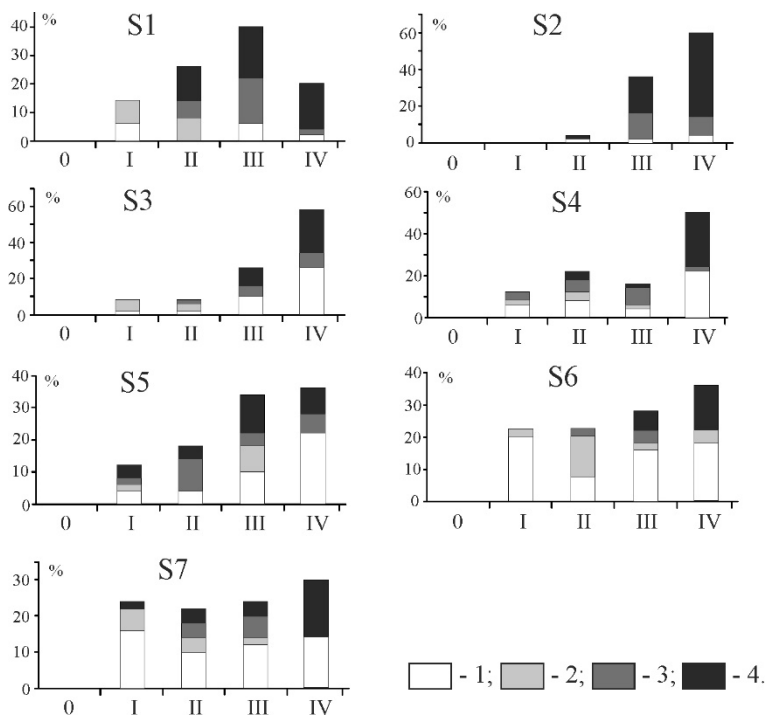
Sampling depth	Sample	Fraction size (mm) / Content (%)					
		Silt and clay	Very fine sand	Fine sand	Medium grained sand	Coarse Sand	Very coarse sand
K-1		<0.09	0.125-0.09	0.25-0.125	0.5-0.25	1-0.5	>1
0.1	S1	31.7	29.2	28.7	9.5	0.7	0.1
0.35	S2	18.7	12.5	32.1	32.2	4.2	0.3
1	S3	18.9	32.3	35.6	11.9	1.2	0.1
1.8	S4	5.9	20.1	56.7	16.4	0.9	0.0
2.3	S5	5.6	13.1	59.9	19.8	1.6	0.0
3	S6	0.6	0.4	1.8	71.5	23.7	1.9
4	S7	0.4	0.5	4.2	46.3	46.9	1.7
NS-6		<0.075	0.10-0.075	0.25-0.125	0.5-0.25	1-0.5	>1
0.3	S1	11.0	6.6	52.7	26.9	2.8	0.0
0.7	S2	0.8	6.8	70.8	18.7	0.4	1.9
1.4	S3	2.0	8.8	65.8	21.2	1.3	0.5
3.2	S4	3.6	8.4	72.8	15.2	0.0	0.0
4	S5	29.9	14.9	50.2	5.1	0.0	0.0
4.2	S6	2.8	0.0	29.4	61.9	5.9	0.0
4.6	S7	26.2	21.1	51.1	1.6	0.0	0.0
5	S8	0.0	0.0	41.1	55.0	3.9	0.0
7.4	S9	1.1	0.1	29.2	52.1	17.4	0.0
9.2	S10	0.5	0.0	29.4	57.5	12.6	0.0
NS-13.14		<0.075	0.10-0.075	0.25-0.125	0.5-0.25	1-0.5	>1
1.1	S1	0.0	0.0	0.6	37.4	58.0	4.0
3.1	S2	8.0	0.0	0.3	36.6	54.2	0.9
3.5	S3	5.9	0.0	10.6	59.9	23.6	0.0
4	S4	0.0	0.0	7.1	62.9	30.0	0.0
4.3	S5	24.4	1.2	15.3	40.9	18.0	0.1
4.75	S6	1.9	0.0	6.5	53.5	37.5	0.6
5	S7	0.0	0.0	8.0	61.5	30.6	0.0
NS-20		<0.09	0.125-0.09	0.25-0.125	0.5-0.25	1-0.5	>1
1.5	S1	0.0	2.2	62.1	21.9	1.3	12.5
3.7	S2	0.0	4.3	72.0	23.0	0.5	0.2
6.5	S3	0.0	4.4	55.8	38.5	1.1	0.3
9.5	S4	0.0	9.3	70.7	16.0	1.5	2.4
16.45	S5	0.0	0.9	56.8	37.6	4.0	0.6
NS-22		<0.09	0.125-0.09	0.25-0.125	0.5-0.25	1-0.5	>1
1.1	S1	0.0	1.4	53.3	44.3	0.9	0.1

920
921
922



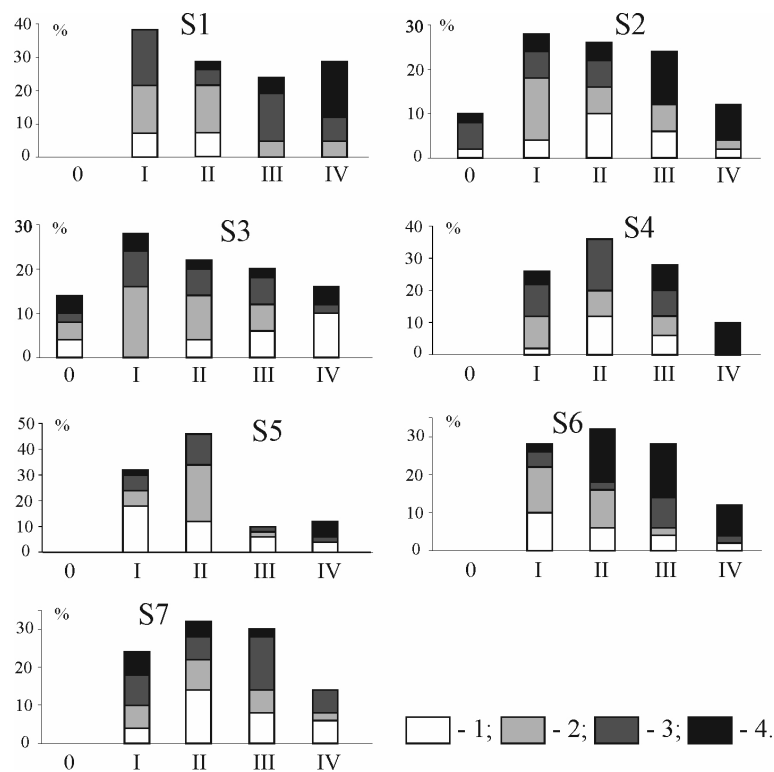
923
924
925
926
927
928

Annex 4. Distribution of quartz sand grains from section NS-6 by roundness and dullness. 1:glossy; 2:quater-matte; 3:half-matte; 4: matte; 0, I, II, III, IV are grades of roundness according to Khabakov scale (1946)

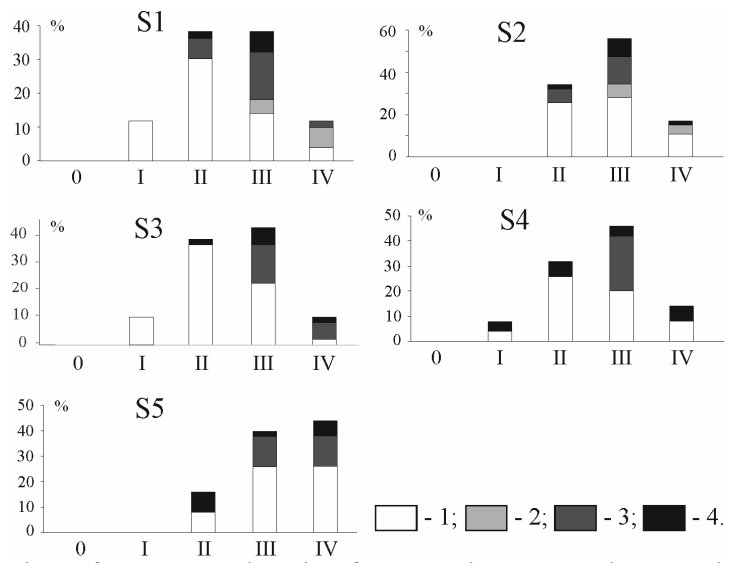


929
930
931
932

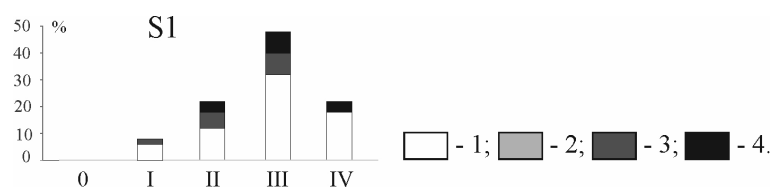
Annex 5. Distribution of quartz sand grains from section NS-6 by roundness and dullness. 1:glossy; 2:quater-matte; 3:half-matte; 4: matte; 0, I, II, III, IV are grades of roundness according to Khabakov scale (1946)



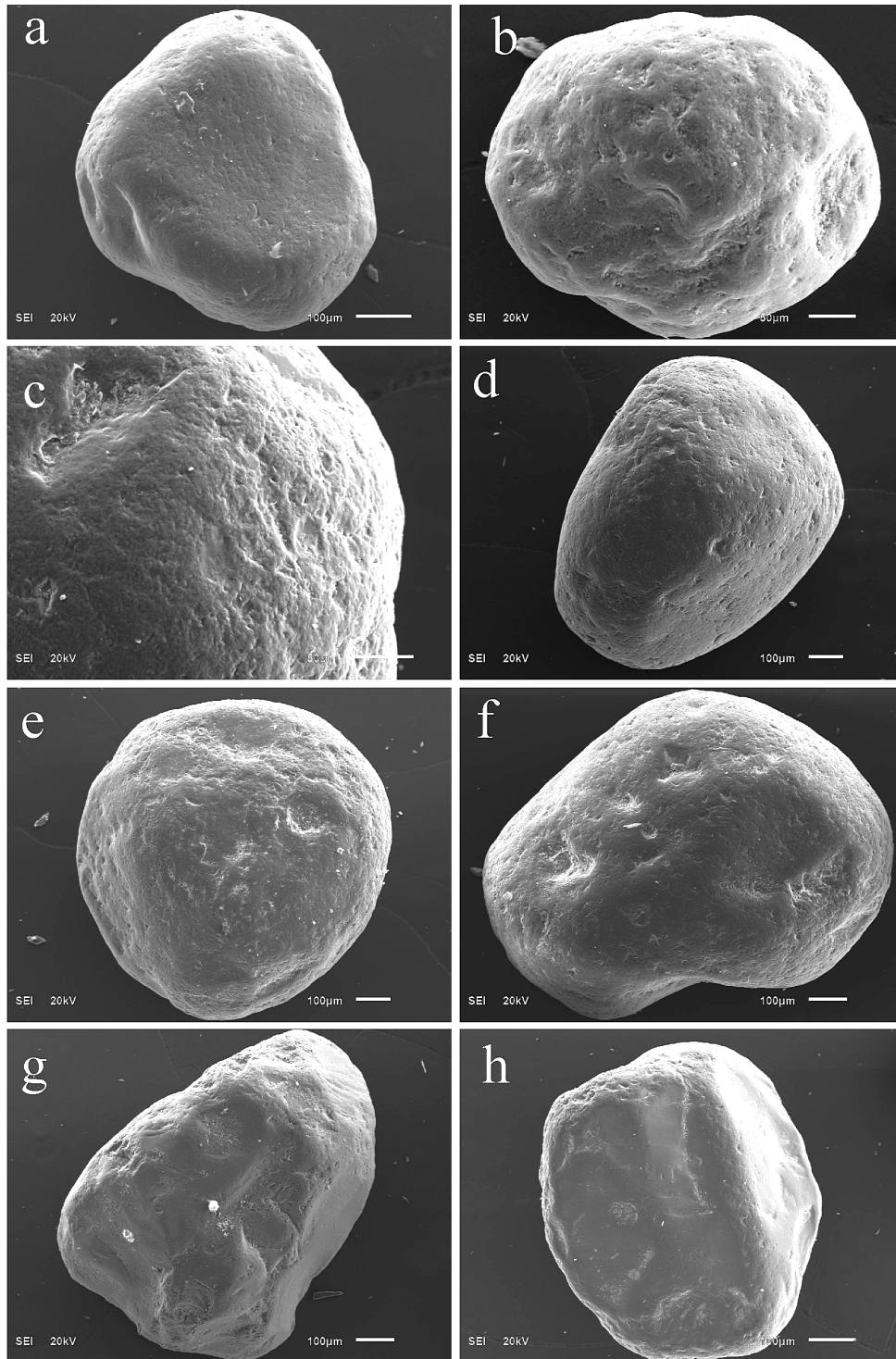
933
934
935
936
937
Annex 6. Distribution of quartz sand grains from section NS-13/14 by roundness and dullness. 1:glossy; 2:quater-matte; 3:half-matte; 4: matte; 0, I, II, III, IV are grades of roundness according to Khabakov scale (1946)



938
939
940
941
942
943
Annex 7. Distribution of quartz sand grains from section NS-20 by roundness and dullness. 1:glossy; 2:quater-matte; 3:half-matte; 4: matte; 0, I, II, III, IV are grades of roundness according to Khabakov scale (1946)



944
945
946
947
Annex 8. Distribution of quartz sand grains from section NS-22 by roundness and dullness. 1:glossy; 2:quater-matte; 3:half-matte; 4: matte; 0, I, II, III, IV are grades of roundness according to Khabakov scale (1946)



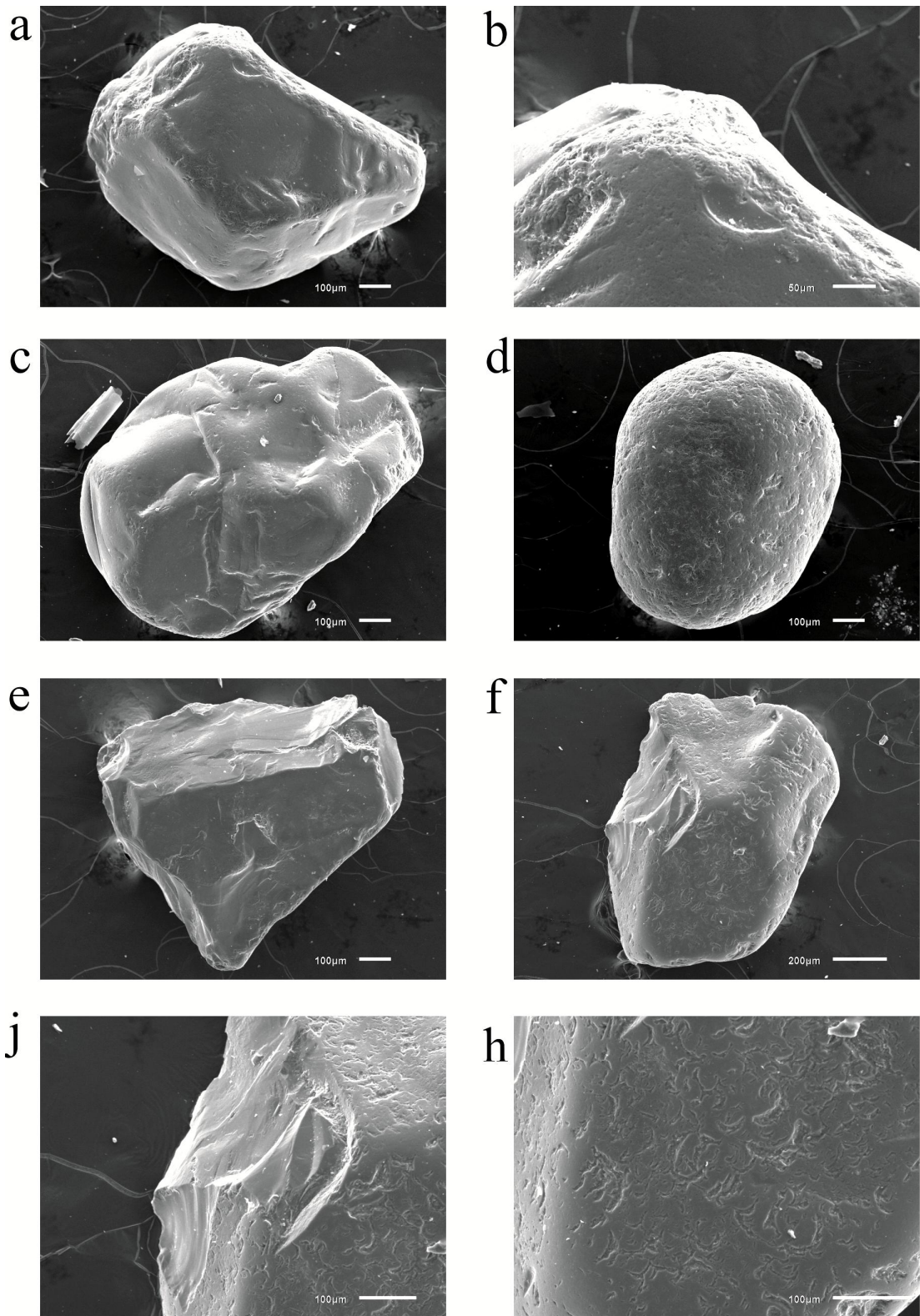
949
 950
 951
 952
 953
 954
 955
 956
 957
 958
 959
 960
 961

Annex 9. SEM photos of quartz grains, section NS-6.

Aeolian sediments: (a): dull grain with a micro-pitted surface and individual crescent-shaped depressions, (b): matte grain with a micro-pitted surface and traces of previous subaquatic treatment.

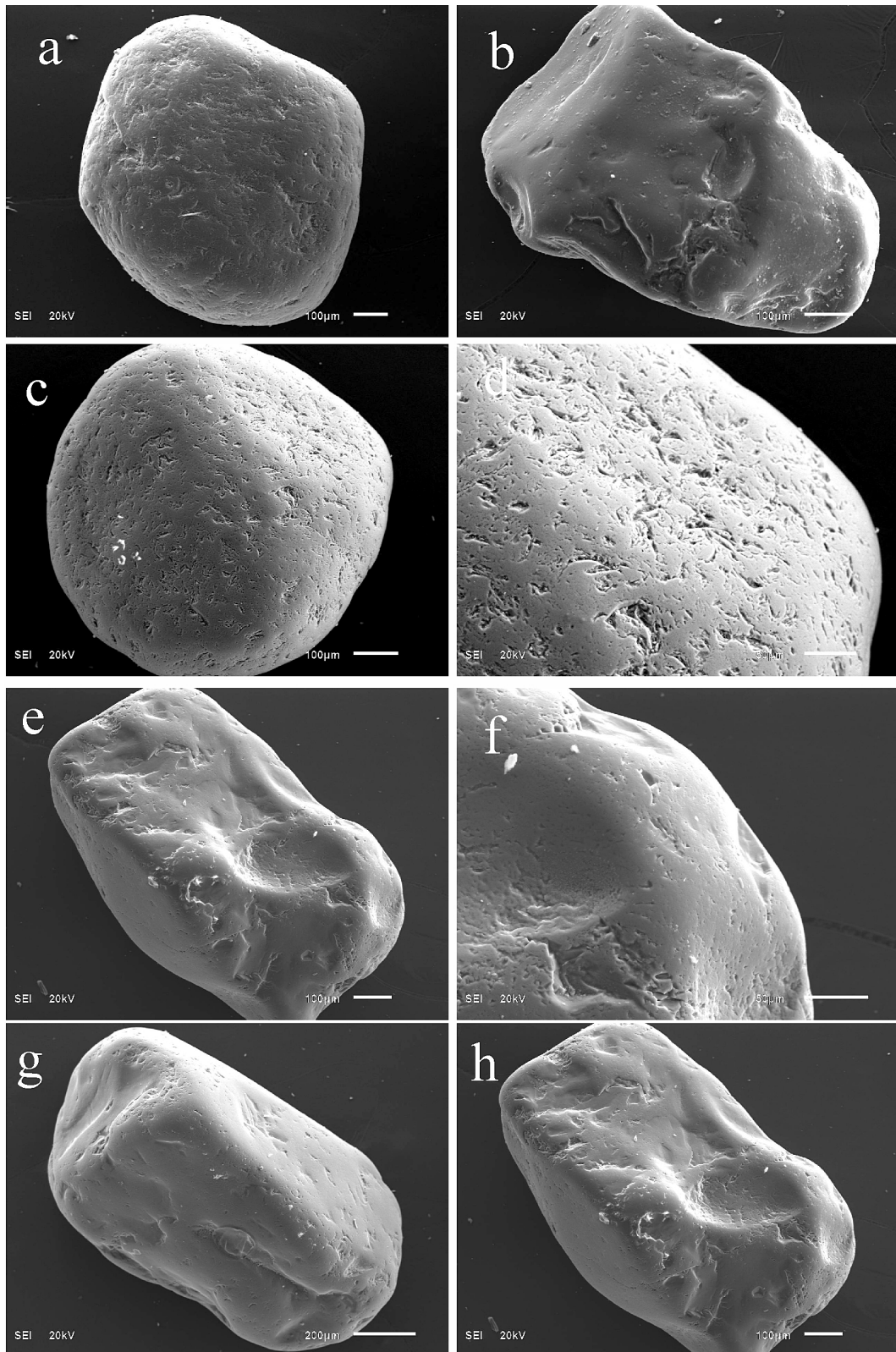
Floodplain sediments: (c): half-matte grain with V-shaped depressions, forming a fine-pitted surface, and with micro-pits, (d): half-matte grain with V-shaped depressions and fine-pitted.

Fluvial deposits: (e): glossy grain with a fine-pitted surface; (f): half-matte grain with a fine-pitted surface and separate V-shaped depressions; (g): glossy grain with fine-pits in the protruding parts of the grain; (h): glossy grain with presedimentation fractures, with the surface subjected to aquatic processes, as expressed by the shape of V-shaped depressions.



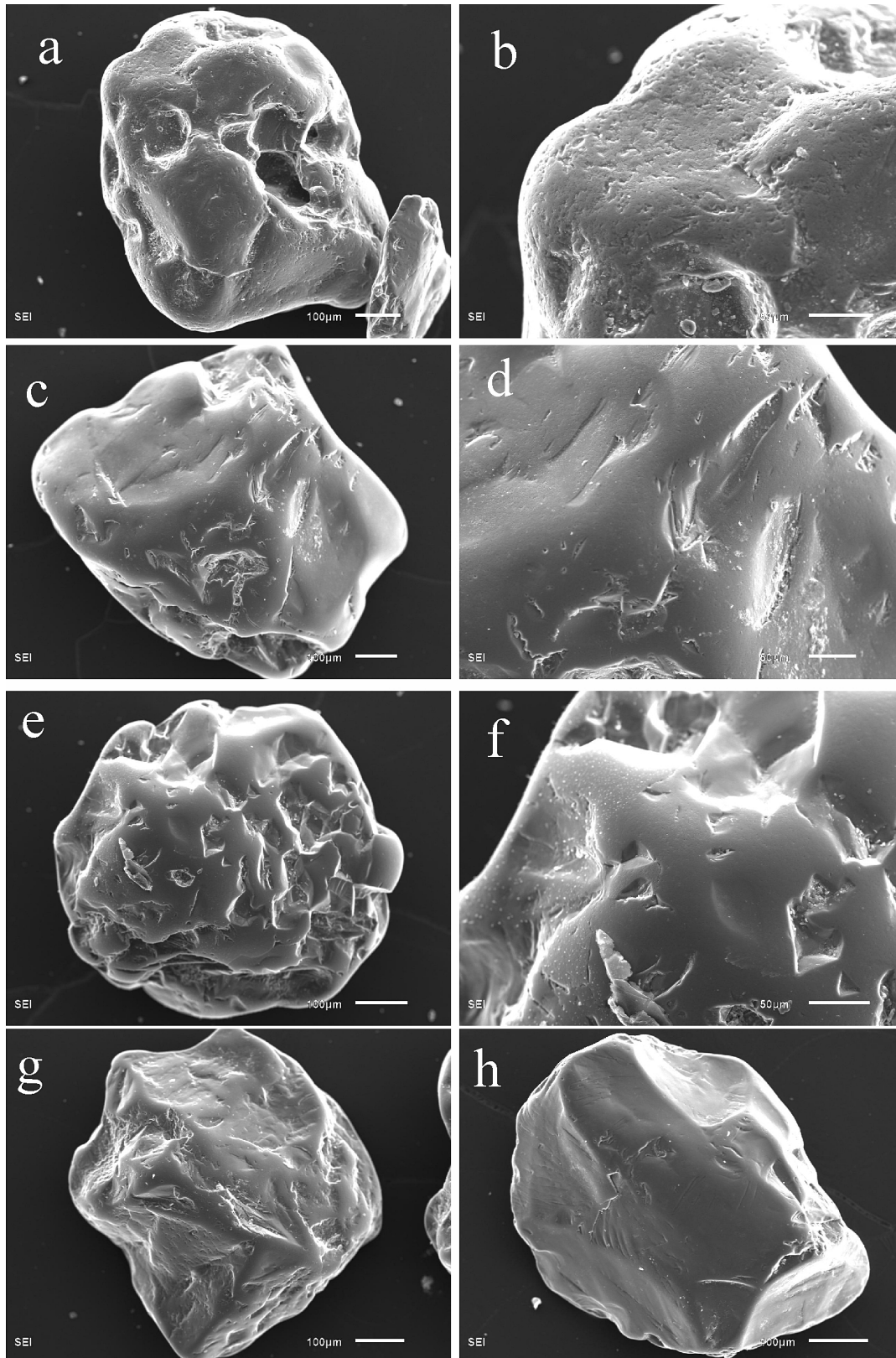
963
 964
 965
 966
 967
 968
 969
 970

Annex 10. SEM photos of quartz grains from S7 section K-1: (a): glossy grain with a smooth surface and flat faces; the faces feature crescentic pits, grain tops feature fine pits; (b): fine-pitted surface of grain 'a'; (c): glossy grain with a smooth surface and sparse fine pits; (d): half-matte grain with fine-pitted surface and crescent pits; (e): glossy grain with flat faces and no evident texture; (f): glossy grain with post-sedimentation conchoidal fractures and crescentic pits; (j): conchoidal fracture of grain 'e'; (h): crescentic texture of grain 'e'.



971
 972
 973
 974
 975
 976
 977
 978
 979
 980

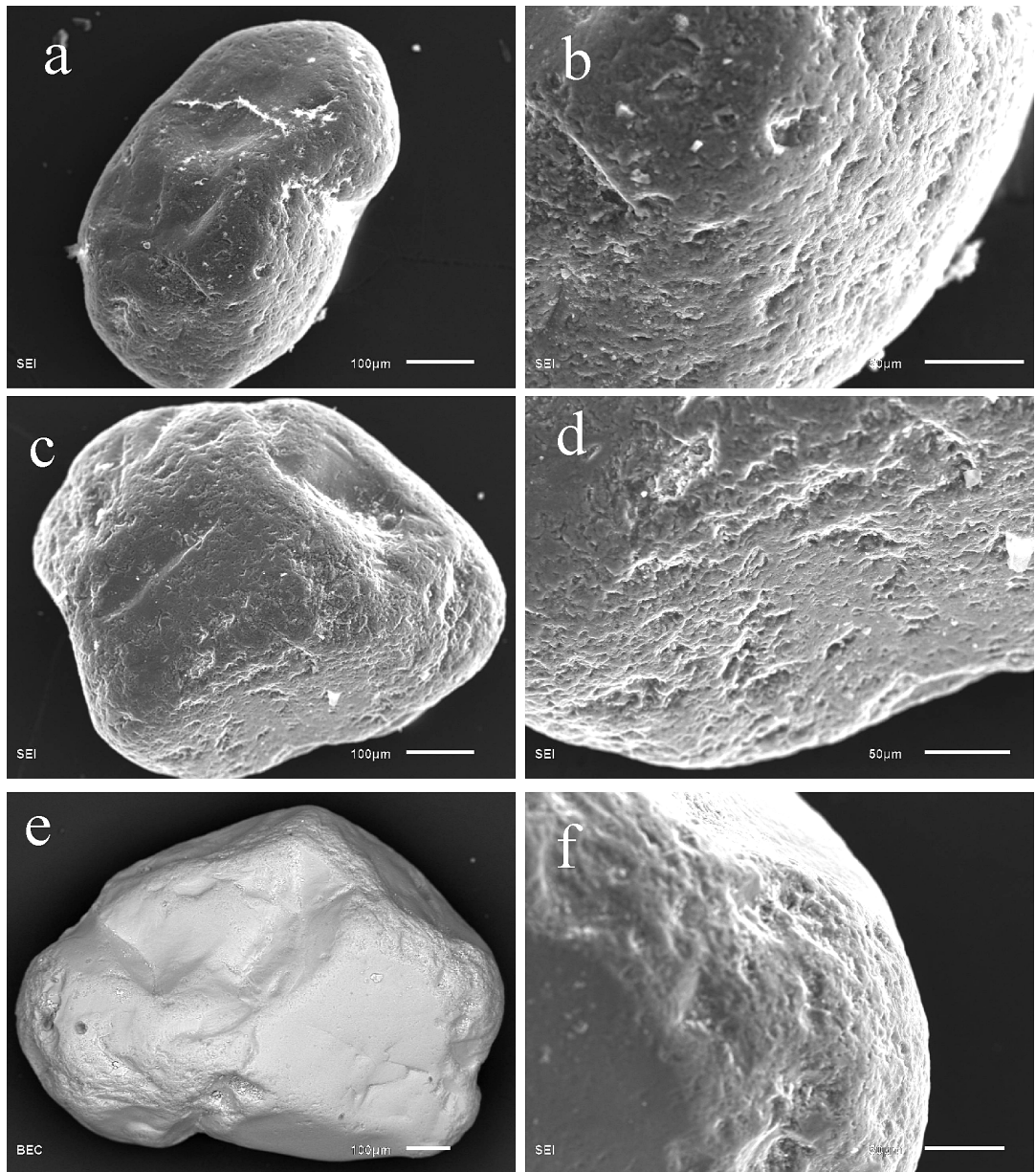
Annex 11. SEM photos of quartz grains from the section NS-13/14: (a) - glossy grain with fine-pitted and crescent and V-depressions, (b): glossy grain of irregular shape with chips and separate V-shaped recesses. Ns14: (c), (d): half-matte grain with a crescentic texture and micropits; (e), (f): glossy grain with chips, V-shapes, and micro-pits on the protruding parts of the grain; (g): half-matte grain of irregular shape with a fine-pitted texture in the protruding parts of the grain; (h): glossy grain with a conchoidal fracture, V-shapes and fine-pits on the protruding parts of the grain.



982
 983
 984
 985
 986
 987
 988
 989

Annex 12. SEM photos of quartz grains from the section NS-20.

(a), (b): matte cavernous grain with a micro-pitted surface and individual crescentic and V-shaped percussions, (c), (d): glossy grain with a smooth surface, grooves, and individual micro-pits, (e), (f): glossy grain with deep groove and single V-shaped percussions, (g): glossy grain of irregular shape with separate V-shaped percussions and a deep-pits, (h): glossy grain with presedimental conchoidal fractures and scratches.



990
 991
 992
 993
 994
 995

Annex 13. SEM photos of quartz grains from the section NS-22.
 (a), (b): glossy grain with a fine-pitted surface, (c), (d): glossy grain with a fine-pitted surface,
 (e), (f): glossy grain with fine-pits on the protruding parts of the grain.